A STUDY OF THE MODERN THEORY OF POLARIZATION ON EXTENSIONS OF ONE DIMENSIONAL TOPOLOGICAL INSULATORS AND DISORDERED SYSTEMS

A THESIS SUBMITTED TO

THE GRADUATE SCHOOL OF ENGINEERING AND SCIENCE

OF BILKENT UNIVERSITY

IN PARTIAL FULFILLMENT OF THE REQUIREMENTS FOR

THE DEGREE OF

MASTER OF SCIENCE

IN

PHYSICS

By

Selçuk Parlak

December 2021

A Study of the Modern Theory of Polarization on Extensions of One Dimensional Topological Insulators and Disordered Systems
By Selçuk Parlak
December 2021

We certify that we have read this thesis and that in our opinion it is fully adequate, in scope and in quality, as a thesis for the degree of Master of Science.

Balázs Hetényi(Advisor)

Oğuz Gülseren

Seçkin Kürkçüoğlu

Approved for the Graduate School of Engineering and Science:

Ezhan Karaşan
Director of the Graduate School

ABSTRACT

A STUDY OF THE MODERN THEORY OF POLARIZATION ON EXTENSIONS OF ONE DIMENSIONAL TOPOLOGICAL INSULATORS AND DISORDERED SYSTEMS

Selçuk Parlak
M.S. in Physics
Advisor: Balázs Hetényi
December 2021

We work on identifying topological and quantum phase transition via the modern theory of polarization. We go through the problem of electrostatics definition of absolute polarization via a discrete chain of anions and cations. We move from this discrete approach to a continuous one and prove the emergence of the Berry phase under adiabatic evolution. Introducing the Resta's position operator, we show the correspondence to the definition of polarization and go through the polarization distribution of the system. Using these concepts we studied band structures, topological invariants, and symmetries in the Su-Schrieffer-Heeger model. With these basics, we analyzed the emergence of torus knots and its identification of topological transition on the distance-dependent SSH model. We go through the formal definitions of knot theory and how to identify them to establish a new system using Klein bottle knots. Following the distance vector structure in the distance-dependent SSH model, we try to establish a real-life system using Klein bottle parametrizations; Pinched torus, figure 8, and the bottle shape. In all of the parametrizations, the interpretation of the real-life system had hoppings on empty sites. Klein bottle knots are tried to observe via parametrizations of the Klein bottle. In all cases, due to the four-dimensional nature of the Klein bottle, we encountered intersecting curves on 3-dimensional interpretations of the Klein bottle. To understand the system better, we go through the Berry phase and dispersion relation of the system. After not encountering anything significant, we try to acquire a knot structure on fundamental polygons. We obtain a Hopf link and unlink with a possible intersection point. The intersection becomes hard to judge due to computational approximation on determining the knot diagrams. Due to the complexity of the project, we go through the Anderson model to study the modern theory of polarization. A background on Anderson localization with

a computational method: Transfer matrix method is given. We state Mott's relation of conductivity and discuss the concept of mobility edge. We show the localization theory of Resta by introducing the complex number z. With this, we prove that the $|z|$ becomes 1 when the states are localized and 0 when we have extended states. We also go through the scaling theory of localization. To understand the scaling theory, we introduce the concept of the renormalization group and discuss how this idea is used in the gang of four paper. We go through the assumptions and results of the gang of four by observing that the scaling exponent of conductance exhibits a critical value only in the three dimensions. Using Resta's quantity, we try to establish the gang of four results by examining the size scaling of the variance of polarization of the system and introducing a renormalization flow with Resta's quantity. We observe the low-temperature limit by examining a single state in the ground state. With this, we recover the results of the gang of four. Based on the discussion of Mott's on mobility edge, we further examine the high-temperature limit, where the system is in the average of all states. We identify the transition point via two fixed points(repulsive and attractive) on flow diagrams and size scaling exponent in all dimensions. We recover the behavior of the gang of four in one and three dimensions by examination of the fixed points, and we state the ambiguity of two-dimensional solutions due to the convergence problem of the fixed points. We further solidify the analogy of conductance and Resta's number by observing the Binder cumulant and analogical mobility edge of the system. We found the same repulsive fixed point on Binder cumulant and analogical behavior on the mobility edge argument.

Keywords: Modern theory of polarization, Disordered systems, Topological insulators, Anderson localization, Polarization distribution.

ÖZET

MODERN POLARİZASYON TEORİSİNİN BİR BOYUTLU TOPOLOJİK YALITKANLARA VE DÜZENSİZ SİSTEMLERE ETKİSİ

Selçuk Parlak
Fizik, Yüksek Lisans
Tez Danışmanı: Balázs Hetényi
Aralık 2021

Modern polarizasyon teorisi yoluyla topolojik ve kuantum faz geçişini tanımlamak için çalışıldı. Mutlak polarizasyonun elektrostatik tanımı problemini, bir anyon ve katyon zinciri aracılığıyla gösterildi. Bu ayrık yaklaşımdan sürekli bir yaklaşıma geçildi ve Berry fazının adyabatik evrim altında ortaya çıktığını kanıtlandı. Resta'nın konum operatörünü polarizasyon ile bağlantısı kanıtlandı ve bir sistemin polarizasyon dağılımı gösterildi. Bu kavramları kullanarak Su-Schrieffer-Heeger modelinde bant yapıları, topolojik değişmezlikler ve simetriler üzerinde çalışıldı. Bu temel bilgilerle, torus düğümlerinin ortaya çıkışı ve mesafeye bağlı SSH modelinde topolojik geçişin tanımlanmasını analiz edildi. Düğüm teorisinin tanımlarından, Klein şişe düğümlerini kullanarak yeni bir sistem kurmaya çalışıldı. Mesafeye bağlı SSH modelindeki mesafe vektör yapısını takiben, Klein şişe parametrelerini kullanarak; sıkıştırılmış torus, figür 8 ve şişe şekli ile gerçek bir fiziksel sistem kurmaya çalışıldı. Tüm parametrelerde, boş kafeslere atlama gözlendi. Klein şişe düğümleri, Klein şişesinin parametreleri yoluyla gözlemlemeye çalışıldı. Her durumda, Klein şişesinin dört boyutlu doğası nedeniyle, Klein şişesinin 3 boyutlu yorumlarında kesişen eğrilerle karşılaşıldı. Sistemi daha iyi anlamak için, Berry aşaması ve sistemin dağılım ilişkisinden geçildi. Önemli bir şeyle karşılaşmadıktan sonra, temel çokgenler üzerinde bir düğüm yapısı elde etmeye çalışıldı. Bir Hopf bağlantısı ve iki bağlantısı kalkmış çember, olası bir kesişim noktasıyla elde edildi. Düğüm diyagramlarındaki kesişim noktası, numerik bir yaklaşımla bulunmaya çalışıldığı için, yorumlaması zorlaştı. Projenin karmaşıklığı nedeniyle, modern polarizasyon teorisini incelemek için Anderson modeline geçildi. Anderson lokalizasyon hakkında bir arka plan, transfer matrisi yöntemi verildi. Mott'un iletkenlik ilişkisini belirtildi ve hareketlilik kenarı kavramını tartışıldı. Resta'nın lokalizasyon teorisini karmaşık

z sayısını tanıtarak gösterildi. Bununla, lokalize durumlarda $|z|$ 'nin 1 ve delokalize durumlarda 0 olduğu kanıtlandı. Ayrıca lokalizasyonun ölçeklendirme teorisinden geçildi. Ölçeklendirme teorisini anlamak için, renormalizasyon grubu kavramı tanıtıldı ve bu fikrin dört insanın yazdığı makalede nasıl kullanıldığı tartışıldı. İletkenliğin ölçeklendirme tabanının sadece üç boyutta kritik bir değer sergilediğini gözlemlendi ve dört insanın varsayımları ve sonuçları incelendi. Resta'nın fikrini kullanarak, sistemin polarizasyon varyansının boyut ölçeklendirmesini inceleyerek ve Resta'nın fikriyle bir renormalizasyon akışı getirerek dört insanın sonuçlarını elde etmeye çalışıldı. Zemin durumunda tek bir durumu inceleyerek düşük sıcaklık sınırını gözlemlendi. Bununla, dört insanın sonuçları incelendi. Mott'un hareketlilik kenarındaki tartışmasına dayanarak, sistemin tüm durumların ortalamasında olduğu yüksek sıcaklık sınırı incelendi. Geçiş noktasını, akış şemaları ve boyut ölçeklendirme kullanılarak tüm sabit boyutlarda iki sabit nokta (itici ve çekici) bulundu. Dört insanın sonuçlarını, sabit noktaları inceleyerek, bir ve üç boyutta kanıtlanıldı ve sabit noktaların yakınsama problemi nedeniyle iki boyutlu çözümlerin belirsizliği belirtildi. Sistemin Binder kümülantı ve analojik hareketlilik kenarını gözlemleyerek iletkenlik benzetmesini ve Resta'nın fikriyle bağlantısı daha da sağlamlaştırıldı. Binder kümülant ve hareketlilik kenarı argümanında analojik davranış üzerinde aynı itici sabit noktayı bulduk.

Anahtar sözcükler: Modern Polarizasyon teorisi, Düzensiz sistemler, Topolojik yalıkanlar, Anderson lokalizasyonu, Polarizasyon dağılımı.

Acknowledgement

First off all, I would like to thank my supervisor Balázs Hetényi. During my research, he made me feel like a colleague rather than his student. He taught me the way of doing research and respected all of my deadlines. I would also like to thank Tahoora (Batoul) Hashemi for discussing and helping with the notions of quantum mechanics as well as supporting me throughout my master journey. Also, I should mention my collegues Yetkin Pulcu and Sertaç Cengiz for the discussions on topological insulators. It would not be an easy subject to grasp without their valueable discussions. I am grateful for the time I spent during pandemic because of my friends, Tahoora Hashemi, Yetkin pulcu and Xhulian Lickollari. I feel lucky to meet such excellent physicists. Finally, I am grateful for having a wonderful family. Their supports, love and patience during this work was immeasurable. I could not thank them enough.

" Localization was a different matter: very few believed it at the time, and even fewer saw its importance; among those who failed to fully understand it at first was certainly its author. It has yet to receive adequate mathematical treatment, and one has to resort to the indignity of numerical simulations to settle even the simplest questions about it."— Philip W. Anderson, Nobel Lecture 1997 [1].

Dedicated to Parlaks...
Hülya, Zafer and Emre.

Contents

List of Figures

List of Tables

Chapter 1

Introduction

The concept of polarization has a long history in the context of physics. Although its definition differs depending on the field of physics, the electric dipole moment was used as the central definition of polarization in electrostatics [9]. However, it is realized that this definition is not well defined in the context of crystalline systems [9]. This problem is not resolved until in the 1990s, Resta and King-Smith and Vanderbilt developed a full theory on the modern approach to the polarization problem [10], [11]. Later on, many applications of the theory started to emerge. In 1997, Resta derived the position expectation value in crystalline systems by the phase of a many body operator acting on the wave function and discussed its relation to the modern theory of polarization [12]. One year later, Resta and Sorella developed a theory on electron localization in crystalline systems based on the modern approach of polarization [13]. In 2000, Resta connected this modern approach to the Berry phase and its connection to topological phase transitions [14]. These developments had a huge impact on both in history of localization and topological insulators.

Localization has a long history, even longer than the theory of polarization in crystalline systems. The first paper that discusses quantum mechanical diffusion in the context of localization was Anderson in 1958[15], [16]. He designed a disordered system and did the first calculations on the absence of diffusion in certain

random lattices. Later on, In 1968, Mott established the localization problem in disordered systems using Kubo-Greenwood's formula. He proposed the concept of mobility edge; a way to interpret the separation of localized and extended states in localization problems[17]. In the 1970s, Thouless and their colleagues, observed the sensitivity of the dc conductivity to boundary conditions in disordered systems [18]. They come up with the Thouless number which became the basis of the formulation of the renormalization group in the context of disordered systems. In 1976, Wegner drew this connection with the corresponding scaling theory of localization [19]. In 1970, Landauer proposed conductance should be the measure of transport through a finite system since the dc conductivity vanishes in a localized system. With the ideas of Thouless, Wegner, and Landauer, in 1979, Abrahams et al. also known as the gang of four, proposed one parameter scaling theory of localization [8]. In this work, they establish the scaling behavior of conductance depending on the size of the system and dimension. The one-parameter scaling even today is hard to argue against. There are been many attempts on testing the one-parameter scaling numerically and experimentally to prove or disprove the localization theory [20],[21], [22], [23], [24]. There are even opposing theoretical papers that argue against the absence of diffusion in two-dimensional disordered systems [25]. But, still the one-parameter scaling paper of the gang of four is widely accepted.

The journey of topological insulators is rather new to the world of condensed matter. It started with the quantum Hall effect experiment. In 1980 Klitzing et al., observed the quantized nature of Hall resistance, and its independence of the geometry of the device [26]. Later on, in 1982, Thouless formulated the discrete nature of the Hall conductance and established it as a topological invariant. One year later, Simon et al. established the connection between Thouless's invariant with Berry phase in quantum adiabatic theorem [27], [28]. Its relation to the topological invariant, Chern number is derived by Kohmoto in 1984. In 1988 Haldane, discovered that it is possible to obtain non-zero discretization of Hall conductance without the need of magnetic field[29]. With these fundamentals, there have been many discoveries on the topological phases of matter. To classify all, in recent years, there has been an urge to complete the table of topological

insulators by classifying them with their symmetries and dimensions [30], [31], [32].

Similarly, in this thesis, we will go through two applications of the modern theory of polarization; a toy topological insulator model and the application of Resta's localization on the Anderson model. In the second chapter of the thesis, a review of the modern theory of polarization is given with its connection to the Berry phase and polarization distribution. In chapter 3, we go through the background of the topological insulators by examining the Su-Schrieffer-Heeger Model(SSH) and the distance-dependent SSH model. After examining the effects of the knot theory and topology on the distance-dependent SSH model, a new topological insulator is introduced based on Klein bottle parametrizations. The chapter is finalized with an extensive knot analysis of the Klein bottle. Chapter 4 starts with a brief introduction to the theories on localization. Background on a localization problem in a disordered tight-binding model known as the Anderson model is given. Background on Mott's and Resta's localization theories is discussed. The chapter ends with the renormalization group and scaling theory of localization. In chapter 5, the numerical application of Resta's localization to the Anderson model is examined. We make an analogical argument based on conductivity discussions on [8] and develop a renormalization flow algorithm. The size scaling exponent of variance of polarization and fixed points of the system are observed. the Binder cumulant and analogical mobility edge of the system are compared to the results of the gang of four. In chapter 5, the main results are summarized.

Chapter 2

Theory of Polarization

2.1 Modern Theory of Polarization

It is well known that electric dipole moment is a measure of the separation of the two oppositely charged particles. Under the assumption of point charges, the polarization in electromagnetic theory is defined through the density of the dipole moment of the system. If you consider a finite linear chain of charges represented with q_i where $i = \{1, 2, .., L\}$, and separation distance of a, one could write the following relation for the definition of polarization,

$$P = \frac{1}{La} \sum_{i=1}^{L} q_i x_i. \tag{2.1}$$

where x_i's are the position of the charge q_i. This approach is well known for finite structures with no periodicity. But in materials, usually, the case is a periodic lattice that is defined by a unit cell. The need for a modern approach to polarization starts with this simple riddle of a lattice model. Let's reconsider the linear chain of anions and cations inside a periodic lattice (fig.2.1). In this case, a problem arises with the definition of polarization under the different choices of unit cells.

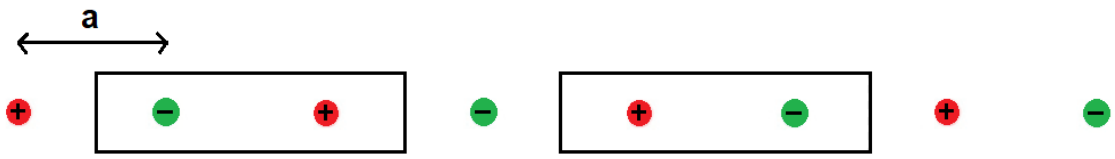

Figure 2.1: Primitive cells of one dimensional anion cation chain.

The two primitive unit cells of the system give different signs of dipole moments. For example, if one sets the coordinate system to the left edge of the unit cell, one can calculate polarization as, in the first unit cell,

$$P = \frac{1}{2a}\left[-q\frac{a}{2} + q\frac{3a}{2}\right] = q. \tag{2.2}$$

In the second unit cell,

$$P = \frac{1}{2a}\left[q\frac{a}{2} - q\frac{3a}{2}\right] = -q, \tag{2.3}$$

where q is the charge magnitude for both the anions and the cations. Obtaining different results by the choice of the unit cell is almost analogous to an ancient mathematical problem known as Grandi's series [33]. In Grandi's series, one could obtain 0 or 1 by the choice of parenthesis of summation(as if a unit cell choice) therefore the series has two solutions. The conclusion of this physical problem is the same, this contradiction clearly shows that the polarization is not well defined in periodic structures. But this is not the only problem with this system. The other major problem is we are acquiring non-zero polarization values in a non-polar system. These two fundamental problems in this basic periodic system is the most basic proof of the need for a modern approach in polarization theory. Now, let's reconsider the same problem when we shift the cations with a distance d(fig. 2.2). This could be considered as an effect of an external electric field. But, the real importance of this step is to experiment on a polar material.

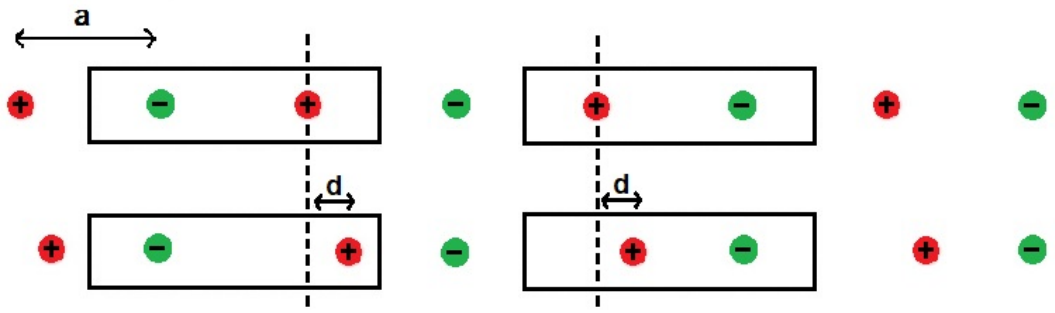

Figure 2.2: Linear chain of anions and cations shifted with respect to the initial system.

Following similar steps, one could acquire the following results for the same choices of unit cells as before, in the first unit cell,

$$P = \frac{1}{2a}\left[-q\frac{a}{2} + q\frac{3a}{2} + qd \right] = q + q\frac{d}{2a}. \tag{2.4}$$

In the second unit cell,

$$P = \frac{1}{2a}\left[q\frac{a}{2} + qd - q\frac{3a}{2} \right] = -q + q\frac{d}{2a}. \tag{2.5}$$

The polarization itself again is not well defined. However, the polarization is shifted by the same value in both unit cells and one could define this as a shift from the initial non-polar system and it is single-valued unlike the polarization itself. This finding drives us to the conclusion that although the polarization itself is not a well-defined quantity in periodic systems, the change of polarization is well-defined [9].

So far, through consideration of discrete simple toy model, we established that the macroscopic theory of polarization does not coincide with its microscopic picture. But, one could take this one step further by considering continuous, real-life systems. To fulfill our goal of understanding the inner mechanism of polarization in real-life experiments, the first question that should be answered is how polarization is measured? The situation in the experiments is not so different from the theory. Generally, polarization itself is measured through a derivative rather than its absolute. For example, one can measure the change of polarization with respect to the field, since it is directly proportional to the susceptibility

[34]. Even in ferromagnetic materials, where the absolute polarization has major importance, the experimental method behind is based on the change of polarization by applying an electric field such that its polarization changes direction. An easy way to measure the change of polarization experimentally is through current density. This current density has a relation through the Maxwell equation;

$$j(t) = \frac{\mathrm{d}P(t)}{\mathrm{d}t}. \tag{2.6}$$

Where j is the macroscopic current density. We could consider this current is produced through a perturbative electric field. Since we are interested in the change of polarization, one can re-write equation 2.6 as,

$$\Delta P = P(\Delta t) - P(0) = \int_0^{\Delta t} j(t)dt. \tag{2.7}$$

It can be seen that, in the adiabatic limit, this integral stays finite, so we could define a formulation through adiabatic evolution. Defining a dimensionless adiabatic time λ, one could write the change of polarization through [34],

$$\Delta P = \int_0^1 d\lambda \frac{\mathrm{d}P}{\mathrm{d}\lambda}. \tag{2.8}$$

Since the change of polarization with respect to time is well defined, the integrand is also well defined. Now that it is possible to measure and calculate the adiabatic change in polarization and it is inherently bulk property insensitive to edges (not dependent on initial and final states rather its change), we can bring the modern solution to the polarization problem.

2.2 Berry Phase

Applying this adiabatic approach to a periodic crystalline system, one would expect that the wave function itself should not undergo a major change. In this system, we adiabatically turn on the vector potential. From this definition, the wavefunction would be a function of this adiabatic time constant λ. Then wave function can be written as a function of its instantaneous eigenstates,

$$|\Psi(\lambda)\rangle = \sum_n C_n(\lambda)|\psi_n(\lambda)\rangle. \tag{2.9}$$

Using the chain rule, Schrödinger equation takes a form,

$$i\hbar\dot{\lambda}\partial_\lambda|\psi(\lambda)\rangle = \hat{H}(\lambda)|\psi(\lambda)\rangle. \tag{2.10}$$

Inserting our initial wavefunction to the Schrödinger equation,

$$i\hbar\dot{\lambda}\big(\sum_n \partial_\lambda C_n(\lambda)|\psi_n(\lambda)\rangle + \sum_n C_n(\lambda)\partial_\lambda|\psi_n(\lambda)\rangle\big) = \hat{H}(\lambda)\sum_n C_n(\lambda)|\psi_n(\lambda)\rangle. \tag{2.11}$$

Projecting this equation to another instantaneous wave function, it is possible the simplify the equation as,

$$C_n'(\lambda)+C_n(\lambda)\langle\psi_n(\lambda)|\partial_\lambda|\psi_n(\lambda)\rangle-\frac{1}{i\hbar\dot{\lambda}}C_n(\lambda)E_n(\lambda)+\sum_{n\neq m} C_n(\lambda)\langle\psi_m(\lambda)|\partial_\lambda|\psi_n(\lambda)\rangle = 0 \tag{2.12}$$

Here we implement the adiabatic approximation. It is possible the ignore the last term, where the state instantaneous state is changing under the adiabatic evolution. This gives an easy integration regime.

$$C_n(\lambda) = C_n(0)\exp\bigg(i\int i\langle\psi_n(\lambda)|\partial_\lambda|\psi_n(\lambda)\rangle d\lambda\bigg)\exp\bigg(\frac{1}{i\hbar}\int\frac{E_n(\lambda)}{\dot{\lambda}}d\lambda\bigg) = C_n(0)e^{i\gamma}e^{i\theta}. \tag{2.13}$$

Then our wave function has a form,

$$|\Psi(\lambda)\rangle \approx \sum_n C_n(0)e^{i\gamma}e^{i\theta}|\psi_n(\lambda)\rangle, \tag{2.14}$$

where,

$$\begin{aligned}\gamma &= \int i\langle\psi_n(\lambda)|\partial_\lambda|\psi_n(\lambda)\rangle d\lambda,\\ \theta &= -\frac{1}{\hbar}\int\frac{E_n(\lambda)}{\dot{\lambda}}d\lambda.\end{aligned} \tag{2.15}$$

This equation shows that after an adiabatic evolution, the wavefunction gains two phases. These phases λ and β are known as geometrical,and dynamical phases respectively. Integrand of the γ is also known as Berry's connection. This emergence of the phases gives an idea of an adiabatically evolving system, but in evolution, we have not yet considered the perturbative field. Turning on the perturbative field, we can impose a new wave function, that approaches the problem more systematically [35],

$$|\psi_n(\lambda)\rangle \to |\psi_n(\lambda)\rangle + \dot{\lambda}|\delta\psi_n(\lambda)\rangle. \tag{2.16}$$

Imposing the linearity with the change of the perturbative field, we recover the instantaneous eigenstates when the perturbative field is constant. It is possible to use this definition in a crystalline system, with Born-von Karman boundary conditions. It is well known that in a crystalline system eigenfunctions are in Bloch form, $\psi_{n\mathbf{k}}(\mathbf{r}) = e^{-i\mathbf{k}.\mathbf{r}}u_{n\mathbf{k}}(\mathbf{r})$, where $\mathbf{k}$ is the wave vector and $u_{n\mathbf{k}}(\mathbf{r})$ is a periodic function with respect to the system size. This eigenvalue problem can be expressed with the hamiltonian $H = p^2/2m + V$, where $H|\psi_{n\mathbf{k}}\rangle = E_{n\mathbf{k}}|\psi_{n\mathbf{k}}\rangle$ or equivalently, $H_{\mathbf{k}}|u_{n\mathbf{k}}\rangle = E_{n\mathbf{k}}|u_{n\mathbf{k}}\rangle$, where $H_{\mathbf{k}} = (\mathbf{p}-\hbar\mathbf{k})^2/2m+V$[34]. Considering this system with the perturbation approach in equation 2.16 into the Schöndinger equation,

$$\begin{aligned} &i\hbar\dot{\lambda}\sum_n(-\langle\psi_{n\mathbf{k}}(\lambda)|\partial_\lambda|\psi_{n\mathbf{k}}(\lambda)\rangle + \frac{1}{i\hbar\dot{\lambda}}E_{n\mathbf{k}}(\lambda))(|\psi_{n\mathbf{k}}(\lambda)\rangle + \dot{\lambda}|\delta\psi_{n\mathbf{k}}(\lambda)\rangle)+ \\ &i\hbar\sum_n\dot{\lambda}\partial_\lambda(|\psi_{n\mathbf{k}}(\lambda)\rangle + \dot{\lambda}|\delta\psi_{n\mathbf{k}}(\lambda)\rangle) = \hat{H}(\lambda)\sum_n(|\psi_{n\mathbf{k}}(\lambda)\rangle + \dot{\lambda}|\delta\psi_{n\mathbf{k}}(\lambda)\rangle). \end{aligned} \tag{2.17}$$

the first order of the perturbation gives,

$$\begin{aligned} &-i\hbar\sum_n\langle\psi_{n\mathbf{k}}(\lambda)|\partial_\lambda|\psi_{n\mathbf{k}}(\lambda)\rangle|\psi_{n\mathbf{k}}(\lambda)\rangle + \sum_n E_{n\mathbf{k}}(\lambda)|\delta\psi_{n\mathbf{k}}(\lambda)\rangle + i\hbar\sum_n\partial_\lambda|\psi_{n\mathbf{k}}(\lambda)\rangle \\ &= \hat{H}(\lambda)\sum_n|\delta\psi_{n\mathbf{k}}(\lambda)\rangle. \end{aligned} \tag{2.18}$$

From this equation we have the perturbation term as,

$$|\delta\psi_{n\mathbf{k}}(\lambda)\rangle = i\hbar\frac{\sum_{m\neq n}\langle\psi_{m\mathbf{k}}(\lambda)|\partial_\lambda|\psi_{n\mathbf{k}}(\lambda)\rangle|\psi_{m\mathbf{k}}(\lambda)\rangle}{E_{m\mathbf{k}}(\lambda) - E_{n\mathbf{k}}(\lambda)}. \tag{2.19}$$

Now the perturbative term of the wavefunction is expressed in terms of the instantaneous wavefunction. The rest is to relate the polarization to the wave function. The simplest way, as mentioned above, is through the current density. Using the continuity equation,

$$\boldsymbol{\nabla}.j = \frac{\partial\rho(\mathbf{r})}{\partial t} = \frac{\partial|\Psi|^2}{\partial t}. \tag{2.20}$$

Taking the time derivative of the density,

$$\dot{\rho}(\mathbf{r}) = \langle\mathbf{r}|\dot{\Psi}\rangle\langle\Psi|\mathbf{r}\rangle + \langle\mathbf{r}|\Psi\rangle\langle\dot{\Psi}|\mathbf{r}\rangle. \tag{2.21}$$

Combining equation 2.21 and Schrödinger equation,

$$\dot{\rho}(\mathbf{r}) = \frac{1}{i\hbar}\langle \mathbf{r}|\hat{H}|\Psi\rangle\langle\Psi|\mathbf{r}\rangle - \frac{1}{i\hbar}\langle \mathbf{r}|\Psi\rangle\langle\Psi|\hat{H}|\mathbf{r}\rangle. \tag{2.22}$$

Here the potential term of the Hamiltonian, cancels out, only the momentum operator remains. Expressing the momentum operator as $-i\hbar\boldsymbol{\nabla}$, one can get

$$\dot{\rho}(\mathbf{r}) = \frac{i\hbar}{2m}\langle \mathbf{r}|\boldsymbol{\nabla}^2|\Psi\rangle\langle\Psi|\mathbf{r}\rangle - \frac{i\hbar}{2m}\langle \mathbf{r}|\Psi\rangle\langle\Psi|\boldsymbol{\nabla}^2|\mathbf{r}\rangle. \tag{2.23}$$

Comparison this equation with the continuity equation, it is possible to conclude that current density is,

$$j(\mathbf{r}) = \frac{i\hbar}{2m}(\langle \mathbf{r}|\boldsymbol{\nabla}|\Psi\rangle\langle\Psi|\mathbf{r}\rangle - \langle \mathbf{r}|\Psi\rangle\langle\Psi|\boldsymbol{\nabla}|\mathbf{r}\rangle). \tag{2.24}$$

This gives as an operator with the consideration of our perturbation gives [35],

$$\hat{j_\lambda} = \frac{i\hbar}{2m}\sum_n(\boldsymbol{\nabla}|\psi_{n\mathbf{k}}\rangle\langle\delta\psi_{n\mathbf{k}}| + \boldsymbol{\nabla}|\delta\psi_{n\mathbf{k}}\rangle\langle\psi_{n\mathbf{k}}| - |\delta\psi_{n\mathbf{k}}\rangle\boldsymbol{\nabla}\langle\psi_{n\mathbf{k}}| - |\psi_{n\mathbf{k}}\rangle\boldsymbol{\nabla}\langle\delta\psi_{n\mathbf{k}}|). \tag{2.25}$$

Taking the expectation value, the current density is,

$$\langle\psi_{n\mathbf{k}}|\hat{j_\lambda}|\psi_{n\mathbf{k}}\rangle = \frac{i\hbar}{2m}(\langle\psi_{n\mathbf{k}}|\boldsymbol{\nabla}|\delta\psi_{n\mathbf{k}}\rangle - \langle\delta\psi_{n\mathbf{k}}|\boldsymbol{\nabla}|\psi_{n\mathbf{k}}\rangle). \tag{2.26}$$

Combining with the equation 2.6, we have the following equality for the derivative of polarization,

$$j_n = \frac{\mathrm{d}P_n}{\mathrm{dt}} = \frac{i\hbar\dot{\lambda}}{(2\pi)^3}\int d\mathbf{k}\sum_{m\neq n}\frac{\langle\psi_{m\mathbf{k}}(\lambda)|\partial_\lambda|\psi_{n\mathbf{k}}(\lambda)\rangle\langle\psi_{n\mathbf{k}}(\lambda)|\hat{p}|\psi_{m\mathbf{k}}(\lambda)\rangle}{E_{m\mathbf{k}}(\lambda) - E_{n\mathbf{k}}(\lambda)} + c.c. \tag{2.27}$$

Using the chain rule, we can get the adiabatic evolution and applying perturbation theory to the hamiltonian $H_\mathbf{k}$ with respect to the $\mathbf{k}$ [34],

$$\frac{\mathrm{d}P_n}{\mathrm{d}\lambda} = \frac{i}{(2\pi)^3}\int d\mathbf{k}\langle\boldsymbol{\nabla}_\mathbf{k}u_{n\mathbf{k}}|\partial_\lambda u_{n\mathbf{k}}\rangle + c.c. \tag{2.28}$$

and integrating both sides with respect to λ yields,

$$\Delta P = \frac{i}{(2\pi)^3}\sum_n\int d\mathbf{k}\langle u_{n\mathbf{k}}|\boldsymbol{\nabla}_\mathbf{k}|u_{n\mathbf{k}}\rangle + c.c. \tag{2.29}$$

This shows a remarkable relation between the berry phase and polarization. Even though a modern approach is obtained for the definition of polarization in periodic systems, we can still expand the definition of polarization through its distribution.

2.3 Polarization Distribution

In periodic boundary conditions, it was established that the absolute polarization was ill-defined. We defined a new modern approach to the problem, but still, even though the polarization is well defined in a periodic lattice, the position operator is not well defined. The key problem is, we want the electrons to be localized within our boundary condition and define the expectation of position that respects the transitional symmetry of the system. To solve this problem, Resta defined the expectation of position as,

$$\langle X\rangle = \frac{L}{2\pi}\mathrm{Im}\log\langle\Psi|\exp\left(\frac{i2\pi\hat{X}}{L}\right)|\Psi\rangle. \tag{2.30}$$

Here, $\hat{X}$ is the total position operator and the exponential acts as a position operator that is modulo of the system size. Resta used this expectation to define the polarization as [12],

$$P = \lim_{L\to\infty}\frac{e}{L}\langle X\rangle = \lim_{L\to\infty}\frac{e}{2\pi}\mathrm{Im}\log\langle\Psi|\exp\left(\frac{i2\pi\hat{X}}{L}\right)|\Psi\rangle. \tag{2.31}$$

To prove this let's reintroduce the Hamiltonian,

$$\hat{H}(k) = \frac{1}{2m}(p-\hbar k)^2 + V. \tag{2.32}$$

It is well established that this hamiltonian, satisfies the eigen value equation,

$$\hat{H}(k)\exp(ik\hat{x})|\Psi_0\rangle = E_0\exp(ik\hat{x})|\Psi_0\rangle. \tag{2.33}$$

To recover the periodicity, k can be defined as 2π/L. Now if we do perturbation theory to order 1/L, $-p\hbar k/m$ term act as a perturbation, giving a correction to the state as,

$$|\Psi_0^{(1)}\rangle = -\frac{2\pi\hbar}{mL}\sum_{m\neq 0}\frac{\langle\Psi_m|\hat{p}|\Psi_0\rangle}{E_0-E_m}|\Psi_m\rangle. \tag{2.34}$$

If we apply use this correction in the eigen value equation 2.33, in the most general case with a added phase γ, we can write the the eigenstate as,

$$\exp(i2\pi\hat{x}/L)|\Psi_0\rangle \approx \exp(i\gamma)\left(|\Psi_0\rangle - \frac{2\pi\hbar}{mL}\sum_{m\neq 0}\frac{\langle\Psi_m|\hat{p}|\Psi_0\rangle}{E_0-E_m}|\Psi_m\rangle\right). \tag{2.35}$$

Inserting this state equation 2.35 into the position expectation that is defined in equation 2.30, and adiabatically evolve time, derivative of the expectation of position is,

$$\frac{d}{dt}\langle X\rangle = \frac{L}{2\pi}\,\mathrm{Im}\left(\frac{\langle\dot{\Psi}_0|\exp(i2\pi\hat{x}/L)|\Psi_0\rangle + \langle\Psi_0|\exp(i2\pi\hat{x}/L)|\dot{\Psi_0}\rangle}{\langle\Psi_0|\exp(i2\pi\hat{x}/L)|\Psi_0\rangle}\right). \tag{2.36}$$

If we substitute the state that is found in equation 2.35, we can get the polarization as,

$$\frac{e}{L}\frac{d}{dt}\langle X\rangle = \frac{ie\hbar}{mL}\sum_{m\neq 0}\langle\dot{\Psi}_0|\Psi_m\rangle\frac{\langle\Psi_m|\hat{p}|\Psi_0\rangle}{E_0 - E_m}|\Psi_m\rangle + c.c. \tag{2.37}$$

This is the exact definition of the current density due to the adiabatic perturbation in equation 2.27. This concludes the proof that this is a correct definition of polarization and position operator. We can use Resta's formulation and expand it to understand the distribution of polarization. Let's define a characteristic function [36],

$$z_q = \langle\psi(x)|\exp\left(i\frac{2\pi\hat{X}}{L}q\right)|\psi(x)\rangle. \tag{2.38}$$

where q is an integer for a periodic system. If we taylor expand the exponential,

$$z_q = 1 + i\frac{2\pi q}{L}\langle\hat{X}\rangle - \frac{1}{2}\frac{(2\pi q)^2}{L^2}\langle\hat{X}^2\rangle + ... \tag{2.39}$$

From this, it is easy to see that the nth cumulants of the polarization can be calculated as,

$$C_n = \left(\frac{L}{2\pi i}\right)^n \frac{d^n\log(z_q)}{dq^n}\bigg|_{q=0}, \tag{2.40}$$

and nth moments as,

$$M_n = \left(\frac{L}{2\pi i}\right)^n \frac{d^n z_q}{dq^n}\bigg|_{q=0}. \tag{2.41}$$

These coincide with the Reta's 1st and 2nd cumulant of polarization and gives a general picture of the polarization through its cumulants. Especially, the second of the polarization has major impacts on the research of insulators which will come more apparent in the following chapters.

Chapter 3

Topological Models

The first observation of topological phases begun with the quantum Hall effect experiment. The effect itself was well known, if you apply an electric field in a linear direction and a magnetic field perpendicular to a 2D sheet of electrons if the magnetic field is strong enough, there is a conductance that is perpendicular to the electric field to counter the Lorentz force [37]. This is what is known to be the Hall voltage. Since the Lorentz force is proportional to the magnetic field, the expectation was that the Hall resistivity would be proportional to the magnetic field, but the results were surprising. Instead of proportionality, they encountered discrete levels of resistivity (or conductivity) and it was quantized to the $\hbar/e^2$ [37]. So, there was no dependence on the shape, impurities, or material of the sample. This was the first topological phenomenon observed. Even though this was just a simple experiment, it lead to great advancement in the knowledge of topological physics and the development of the field of topological insulators.

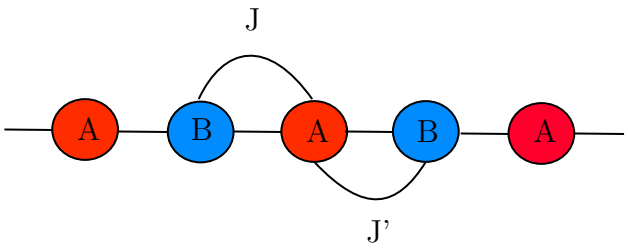

Figure 3.1: SSH model with sites A and B with nearest neighbor hoppings J and J'.

3.1 The Su-Schrieffer-Heeger Model

The most known topological toy model is the Su-Schrieffer-Heeger model named after their writers Su, Schrieffer, and Heeger and abbreviated with their initials(SSH). Even though it is a simple tight-binding model, the model itself shows all the topological properties that a system can have. It is a one-dimensional system with N sites, each unit cell containing sites A and B with alternating hopping amplitudes. Ignoring the electron interaction, this system can be expressed with the Hamiltonian,

$$H = J\sum_{n=1}^{L}(c_n^+ d_n + h.c.) + J^{'}\sum_{n=1}^{L-1}(c_n^+ d_{n+1} + h.c.), \tag{3.1}$$

where c_n, d_n and c_n^+, d_n^+ are second quantization annihilation and creation operators for the site A and B respectively [38].

If we adopt periodic boundary conditions, we can use the Bloch function to solve the Schödinger equation. Taking the Fourier transform of the second quantization operators,

$$\begin{aligned} c_n &= \frac{1}{\sqrt{L}}\sum_k c_k e^{ikn} \\ d_n &= \frac{1}{\sqrt{L}}\sum_k d_k e^{ikn}, \end{aligned} \tag{3.2}$$

one arrive at the following Hamiltonian,

$$H(\mathbf{k}) = \sum_k J(c_k^+ d_k + h.c.) + J^{'}(c_k^+ d_k e^{ik} + h.c). \tag{3.3}$$

Then bulk Hamiltonian can be defined as,

$$H = \sum_k H(\mathbf{k}) = \sum_k \mathbf{d}(k) \cdot \vec{\sigma} = \sum_k [d_x(k)\sigma_x + d_y(k)\sigma_y + d_z(k)\sigma_z] \tag{3.4}$$

where $(\sigma_x, \sigma_y, \sigma_z)$ are Pauli matrices, and the distance vector becomes,

$$\begin{aligned} d_x(k) &= J + J' \cos(k), \\ d_y(k) &= J' \sin(k), \\ d_z(k) &= 0, \end{aligned} \tag{3.5}$$

with the dispersion relation,

$$E(k) = \pm\sqrt{J^2 + J'^2 + 2JJ' \cos(k)}. \tag{3.6}$$

Realize the magnitude of the distance vector gives the energy dispersion. As wavenumber k changes, due to the periodicity of the bulk space hamiltonian, the distance vector traces out a closed-loop on dx, dy plane. To describe an insulator, we should avoid the origin since crossing the origin gives extended states. To understand the topological invariant, in this case, I can adiabatically deform this closed loop. If the closed-loop contains the origin, since I cannot pass through it without closing the gap, this defines a distinct topological phase in comparison to not winding the origin. This topological invariant is called the winding number, and it is a measure of how many times this distance vector winds around the origin [38]. One could understand this better if we plot the dispersion relation and distance vector of the SSH model. If we plot this dispersion relation with respect to different hopping ratios, one could get the gap closure when the hopping parameters are equal.

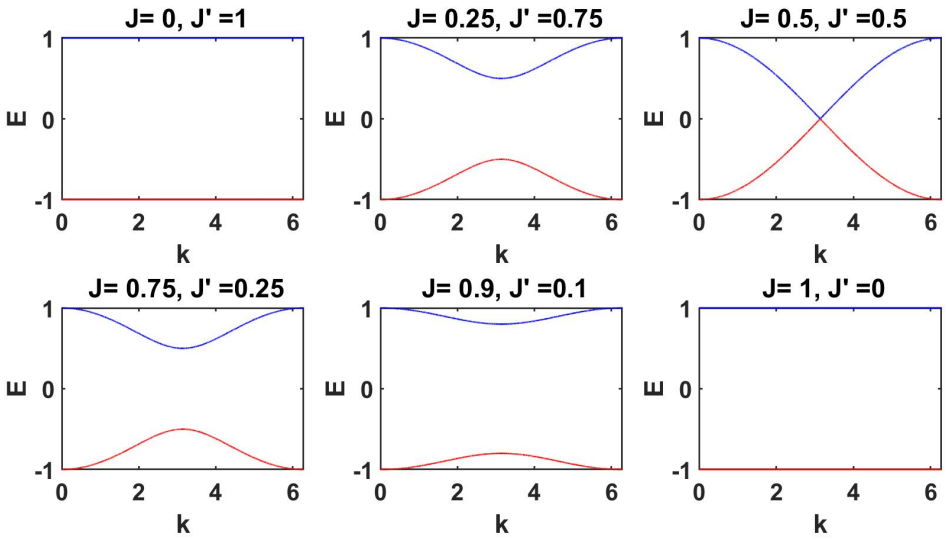

Figure 3.2: Energy band structure of SSH with hoppings J and J', where k is from 0 to 2π.

The behavior of the energy band seems to be quite symmetric, but, considering the previous discussion on winding number, closing the bulk should correspond to a topological shift(fig. 3.2). This topological transition is hard to see through the energy dispersion, however, it can be seen through the distance vector. If we plot our distance vector, it can be seen that after the critical value, when the gap closes and our system becomes conductor, the winding number of the system changes, and this change cannot be reverted back without closing the gap again(fig. 3.3).

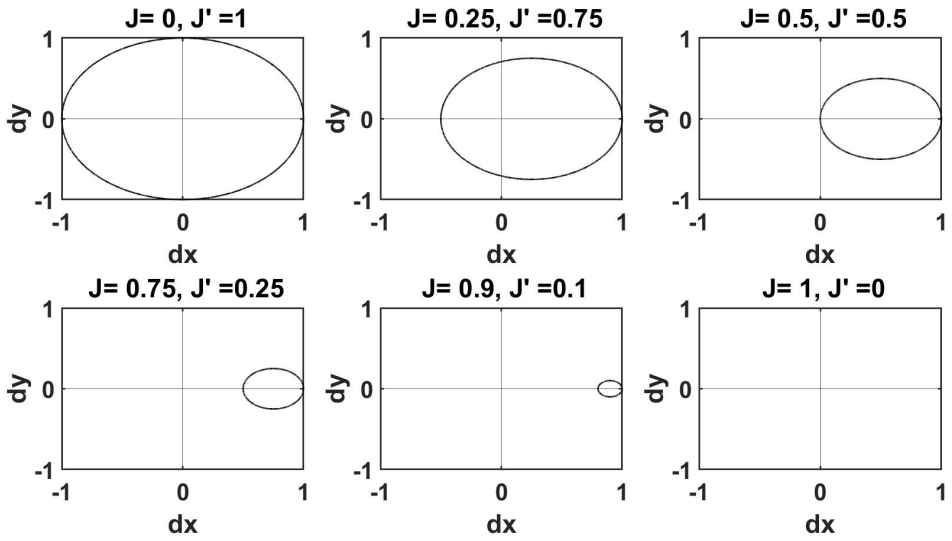

Figure 3.3: Distance vector of SSH with hoppings J and J', where k is from 0 to 2π.

This shows a topological transition that is defined through the winding number. However, this is not the only topological invariant in this system. Since we consider a deformation process, one could suggest this deformation can be done adiabatically. Adiabatically deforming a system, reminds the discussion of polarization. Can polarization be a topological invariant? The short answer to this question is yes. The basic reason behind that is, the Berry phase itself is a topological invariant since it can be defined on a closed-loop in k space. Since our vector $\mathbf{d}(k)$ sweeps a closed loop on the Bloch surface, the Berry phase can be defined as the solid angle of the loop[39]. The basic consequence of this is that the Berry curvature integrated over the Brillouin zone, similar to the winding number, gives how many times the vector $\mathbf{d}(k)$ winds the Bloch sphere. This gives the topological invariant Chern number [39]. But, more importantly, this adiabatic approach shows that the Berry phase and consequently the polarization of the system are topological invariants.

3.2 Symmetries of the System

Symmetries have always been a major part of physics. In almost all physical problems, imposing certain symmetries to the system, either reduces the analytical work or changes the outcome. In topological insulators, the situation is not so different. The topological insulators are classified by the three main symmetries, time reversal(T), particle-hole(C), and chiral(S). Time reversal and particle-hole symmetry operators squares to either -1 or 1, while for the chiral symmetry only possible value is 1 [40]. These results in 10 different symmetry classes. Since materials can be represented with these ten symmetry classes, this is called the ten-fold way.

Symmetry				Spatial Dimension d								
Class	T	C	S	1	2	3	4	5	6	7	8	$\cdots$
A	0	0	0	0	$\mathbb{Z}$	0	$\mathbb{Z}$	0	$\mathbb{Z}$	0	$\mathbb{Z}$	$\cdots$
AIII	0	0	1	$\mathbb{Z}$	0	$\mathbb{Z}$	0	$\mathbb{Z}$	0	$\mathbb{Z}$	0	$\cdots$
AI	1	0	0	0	0	0	$\mathbb{Z}$	0	$\mathbb{Z}_2$	$\mathbb{Z}_2$	$\mathbb{Z}$	$\cdots$
BDI	1	1	1	$\mathbb{Z}$	0	0	0	$\mathbb{Z}$	0	$\mathbb{Z}_2$	$\mathbb{Z}_2$	$\cdots$
D	0	1	0	$\mathbb{Z}_2$	$\mathbb{Z}$	0	0	0	$\mathbb{Z}$	0	$\mathbb{Z}_2$	$\cdots$
DIII	-1	1	1	$\mathbb{Z}_2$	$\mathbb{Z}_2$	$\mathbb{Z}$	0	0	0	$\mathbb{Z}$	0	$\cdots$
AII	-1	0	0	0	$\mathbb{Z}_2$	$\mathbb{Z}_2$	$\mathbb{Z}$	0	0	0	$\mathbb{Z}$	$\cdots$
CII	-1	-1	1	$\mathbb{Z}$	0	$\mathbb{Z}_2$	$\mathbb{Z}_2$	$\mathbb{Z}$	0	0	0	$\cdots$
C	0	-1	0	0	$\mathbb{Z}$	0	$\mathbb{Z}_2$	$\mathbb{Z}_2$	$\mathbb{Z}$	0	0	$\cdots$
CI	1	-1	1	0	0	$\mathbb{Z}$	0	$\mathbb{Z}_2$	$\mathbb{Z}_2$	$\mathbb{Z}$	0	$\cdots$

Figure 3.4: Tenfold symmetry of topological insulators with respect to dimensions. Adapted from [2].

There are three topology classes, hence three entries. The most trivial one is when the entry is 0. This means there is no topological transition in the material so materials can deform to the other zero-entry materials without closing the gap and breaking the symmetries. The entry Z, corresponds to integer values $0, \pm 1, \pm 2, ...$ for the topological invariant, while the entry Z_2, is either 0 or 1, corresponding to two distinct topological phases [2]. This means the topological

behavior of every material can be determined through its symmetries and the topology class of the material can be changed by imposing certain symmetries or changing its dimension.

3.2.1 Time Reversal Symmetry

Time reversal symmetry, as it guesses by its name, is defined to answer the question of what happens to the system if I move backward in time. This was a known concept in classical physics. If I reverse the time in a mechanical system, an object moving in time must change its direction, keeping the same velocity and displacement. This suggests a change in momentum while keeping the position the same. Although classically, this definition is sufficient, in quantum mechanics we encounter a problem in the canonical commutation relation,

$$[x, p] = i\hbar. \tag{3.7}$$

In this case, if we apply the classical time-reversal operator, the canonical commutation no longer holds (eq. 3.8).

$$T[x, p]T^{-1} = -[x, p]. \tag{3.8}$$

The solution came from Eugene Wigner. He showed that the time-reversal operator must be anti-unitary, where the operator is expressed by a unitary and a conjugation operator, namely,

$$T = UK, \tag{3.9}$$

where U and K are the unitary and conjugation operator respectively. From this definition, it is possible to show that every anti-unitary operator has the following property,

$$T^2 = UKUK = UU^* = U(U^T)^{-1}. \tag{3.10}$$

If we use the fact that, taking the time reversal of a system twice, the system goes back to the inital state up to a phase shift suggests that T^2 must be diagonal phase matrix[41]. This suggests transpose of the T^2 is itself, or equivalently $T^2U^T = U$ and $U^T = UT^2$. This leads to the equation,

$$T^2UT^2 = U. \tag{3.11}$$

If we take the expectation value of equation 3.11, it is clear that T^2 is either 1 or -1 as discussed at the beginning of the chapter. We say a Hamiltonian H is time-reversal symmetric if,

$$THT^{-1} = H, \tag{3.12}$$

[40].

3.2.2 Partile Hole Symmetry

In general, when we deal with a condensed matter system, it is convenient to think of a half-filled (Fermi level) system rather than one electron system. Removing an electron below the Fermi level creates a hole. So, one could say annihilation of an electron can be considered as the creation of a hole if the energy spectrum is symmetric $\epsilon_k = \epsilon_{-k}$, where ϵ_k is the energy of a single particle. This symmetry of electronic gas naturally shows itself in superconductor and bipartite topological insulators. In superconductors, this operator has a form of $C = \sigma_i K$, where σ_i is a Pauli matrix. Due to its anti-unitary nature, it has the two possible values for C^2 as in the time-reversal operator. One system has particle-hole symmetry if the Hamiltonian of the system satisfies,

$$CHC^{-1} = -H, \tag{3.13}$$

[40] [42].

3.2.3 Chiral Symmetry

Chiral symmetry is dependent on the time-reversal and particle-hole symmetry $S = TC$ .This relation suggests two possibilities for the existence of chiral symmetry, either both time-reversal and particle-hole symmetries exist or both of them are missing. More technically, we say a system is a chiral symmetric if it satisfies,

$$SHS = -H, \tag{3.14}$$

[40]. Chiral operator is both Hermitian and unitary, resulting in S^2 to be 1.

3.2.4 Symmetries of the SSH model

It is already mentioned that the SSH model is the simplest topological insulator. Now, one would be curious in which category of topological insulator the model is in? We actually trivially know the answer from the fact that it has already been established it has two topological phases so it must be either Z_2 or Z topological insulator. To find out let us establish the operators that correspond to these symmetries. For the time-reversal, one could see $T = 1K$ is a valid operator for time-reversal since,

$$TH(k)T^{-1} = K\bigg((J + J'\cos(k))\sigma_x + J'\sin(k)\sigma_y\bigg)K = H(-k). \tag{3.15}$$

The reversal is momentum $-k$ was expected due to time reversal. Similarly for the particle-hole symmetry, one could try a similar operator that is used in superconductors $C = \sigma_z K$, then,

$$CH(k)C^{-1} = \sigma_z K\bigg((J + J'\cos(k))\sigma_x + J'\sin(k)\sigma_y\bigg)K\sigma_z = -H(-k). \tag{3.16}$$

Again, -k is due to the electron-hole pair as mentioned above. Then using these symmetries Chiral symmetry can be found to be,

$$S = TC = K\sigma_z K = \sigma_z^* = \sigma_z. \tag{3.17}$$

It is trivial to see that this operator satisfies equation 3.14. Since, time reversal and particle-hole symmetry squares to 1, this gives the BDI system for this model in 1D, giving a Z type topological insulator. However, although this argument is true, the meaning of the periodic table goes beyond this simple observation. We could also consider the SSH model in other classes. The hidden meaning of the table answers the question, what kinds of perturbations can I add to the system without breaking its topology? For example, one could perturb the SSH system with AIII symmetry class without breaking the Z class of the topological insulator, since AIII symmetry class in 1D represents the Z type topological insulators.

3.3 Distance Dependent SSH to Klein Bottle Model

SSH model, even though a toy topological model, entails the fundamentals of topological insulators. The simple nature of it awakened the urge to the observation of the quantities of this model to understand how this model can be extended or generalized to explain a more complicated system in a simple toy model. With the knowledge of the periodic table of topological insulators, there are been many extensions of SSH models with different onsite potentials, hopping parameters or external fields.

3.3.1 Distance Dependent SSH

One of the examples of this toy model was recently published by Balazs Hetenyi et al. The model separates the sites A, B with a rational distance $r = p/q$ and introduced next neighbour interaction with complex hopping. This results in Z_2 topological insulator with two distinct topological phases. With these constraints, the models start with the SSH model with second neighborhood interactions,

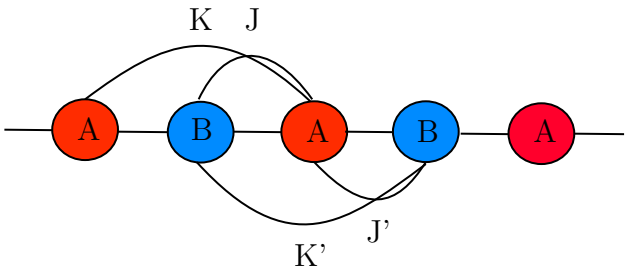

Figure 3.5: SSH Model with sites A and B including nearest neighbor hopping J and next-nearest neighbor hopping K.

$$H = \sum_{n=1}^{L} J c_n^+ d_{n-1} + J^{'} c_n^+ d_n + K c_n^+ c_{n-1} + K^{'} d_n^+ d_{n-1} + H.C.. \tag{3.18}$$

Here, the distance dependence take place, when we take the Fourier transform of the operators, after the transform the Hamiltonian becomes,

$$H_k = c_k^+ d_k e^{-ik(1-p/q)} + J^{'} c_k^+ d_k e^{ikp/q} + K c_k^+ c_k e^{-ik} + K^{'} d_k^+ d_k e^{-ik} + h.c \quad (3.19)$$

In order to break the time-reversal symmetry, we could take K to be complex. This gives the Hamiltonian,

$$H(k) = \begin{pmatrix} 2K \sin k & Je^{ikp/q} + J'e^{-ik(1-p/q)} \\ Je^{-ikp/q} + J'e^{ik(1-p/q)} & -2K \sin k \end{pmatrix}. \quad (3.20)$$

Using the Pauli matrices, we could find the distance vector of this Hamiltonian to be,

$$\begin{aligned} d_x(k) &= J \cos\left(\frac{kp}{q}\right) + J' \cos\left(k\left(1 - \frac{p}{q}\right)\right), \\ d_y(k) &= -J \sin\left(\frac{kp}{q}\right) + J' \sin\left(k\left(1 - \frac{p}{q}\right)\right), \\ d_z(k) &= 2K \sin(k). \end{aligned} \quad (3.21)$$

The interesting behavior of this system shows itself in this distance vector. Plotting this distance vector before, in, and after gap closure gives different knot structures. Although it does not gives the distinction between topological trivial and non-trivial phases, the knots identify the topological transition (fig. 3.6) [3].

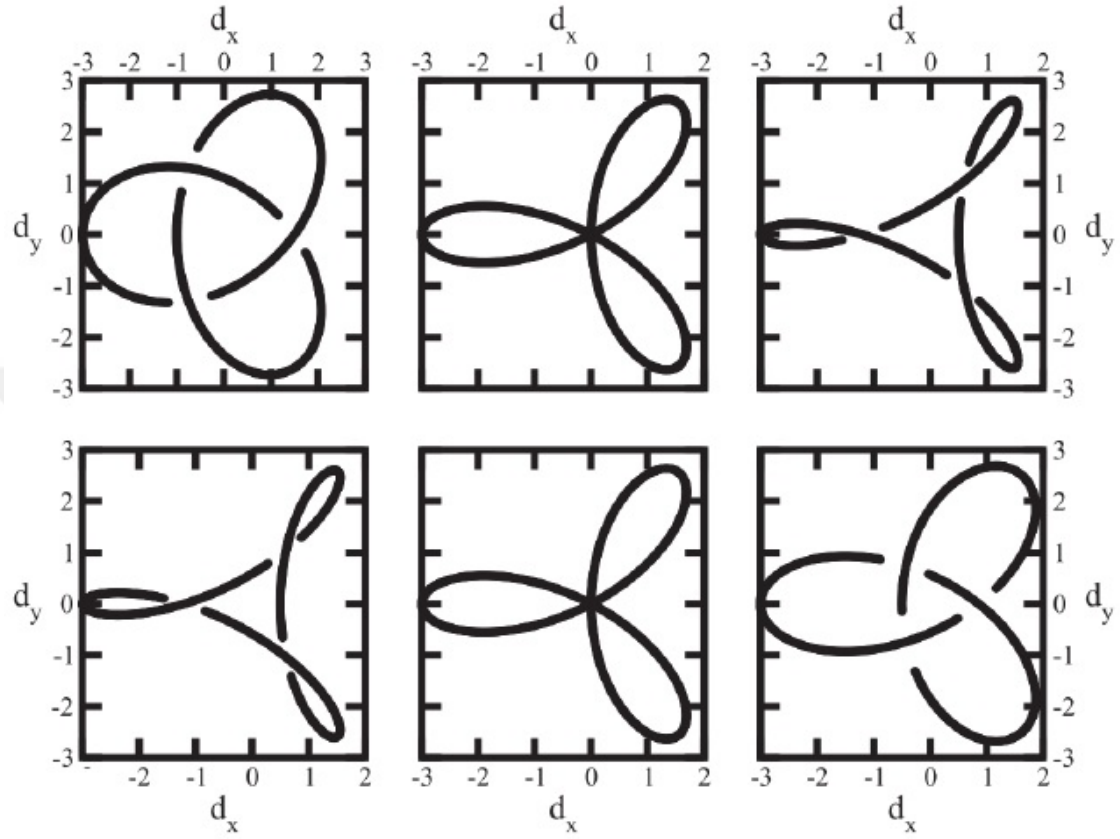

Figure 3.6: The topological transition of the distance-dependent SSH model. The transition from a trefoil knot to an unknot represents the topological transition. Adapted from [3].

The rational distance also change the number of crossing points in the knot. Since the value q is associated with the crossing point, if we increase it, a well-known topological shape emerges that is known as torus knot. The reason behind this is that torus has a similar two-parameter (p,q) parametrization. This draws an interesting parallel to the knot theory and how the knots are related to a family of a topological shape. To understand the basics of this, one must go through the knot theory.

3.4 Knot Theorem

The knot theorem starts with the identification of a knot. A knot is defined through a closed curve with no intersection that cannot be unraveled to an unknot (circle). One of the well-known examples of a knot is a trefoil knot that emerges in the extended SSH model (fig. 3.6). The knots are represented by x_y, where x is the number of crossing points (3 for the trefoil knot) and y is the uniqueness of the knot, meaning that the number of prime knots that exists with the crossing number x (1 for the trefoil knot) [4]. This means that any other knot other than the prime ones can be reduced to a prime knot by applying what is known to be Reidemeister moves.

3.4.1 Reidemeister moves

Working on the diagrams of knots, J. W. Alexander and Garland Baird Briggs, and independently Kurt Reidemeister discovered that knots can be resolved or can be related to one another with a sequence of three moves [43] [4], [**?**]. If two knots are said to be the same then one can apply the Reidemeister moves to one knot to convert into the other. There are three Reidemeister moves, however, sometimes a zeroth move can be seen in literature but this move is not considered as Reidemeister moves since it basically says you can change the curve without changing the crossing number. The rest of the moves can straightforwardly be explained as following manner. The first move is the unfolding of a curve, the second is the separation of the curve and the third one is the changing direction of the curve without changing its crossing number (fig.3.7) [4].

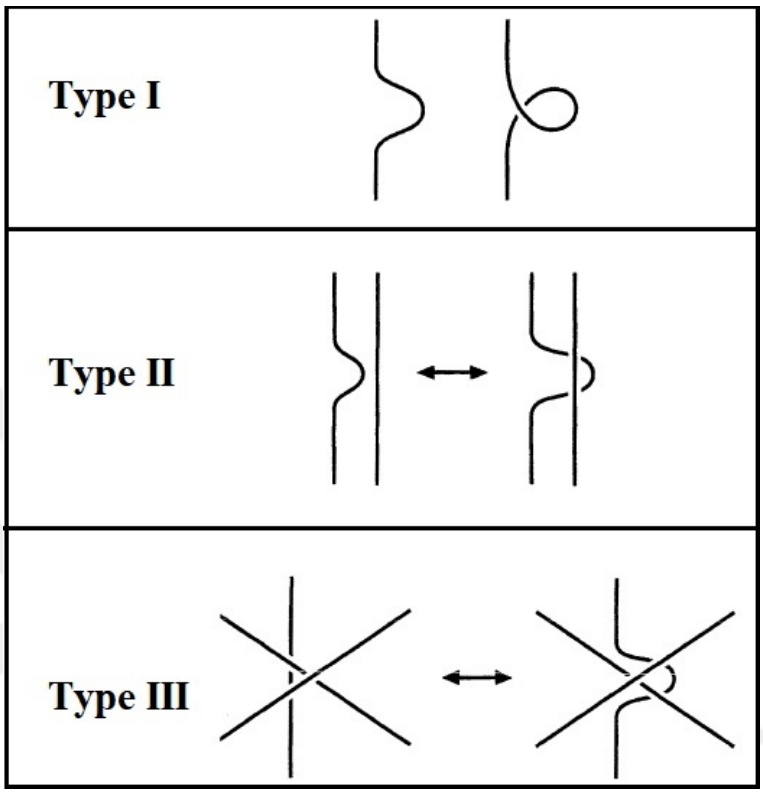

Figure 3.7: The table of the Reidemeister moves. Adapted from [4].

These moves can be used to identify the knots in our physical models. If we look at our previous distance vector that resulted in knot diagrams (fig. 3.6), it is possible to see when the intercell and outer cell hopping differs from each other, either we can acquire unknot by applying Reidemeister moves or we get a trefoil knot which cannot be reduced to unknot by applying the Reidemeister moves. This is one way to distinguish simple knots. But, when the knot diagrams are much more complex, we need a more analytical way to calculate the class of the knot.

3.4.2 Alexander polynomial

To understand more complex knots, one way to commute the problem is with what is known as Alexander polynomial. This polynomial is known to be knot

invariant, which basically means a knot has a unique representation in form of a polynomial and it is invariant under the Reidemeister moves. In Alexander polynomial, the basic idea is to give an orientation to a knot and define a matrix through assigning variables to crossing points and the arcs of the knot [4].

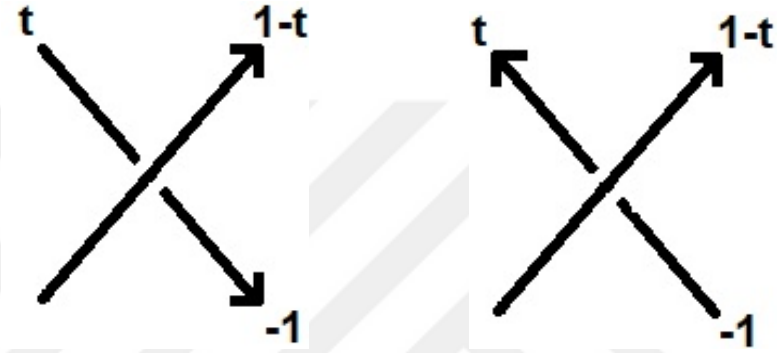

(a) (b)

Figure 3.8: The algorithm on left-handed (a) and right-handed (b) knot crossings with given direction to construct Alexander matrix.

Due to the nature of orientation, there are two possible crossing points one could encounter, which are similar to the right hand rule encountered in electrodynamics systems. The direction of the thumb shows the direction of the upper arc represented with 1-t and the curving direction takes the parameter -1 or t depending on the direction as it can be seen in figure 3.8 [4]. Therefore, in order to construct the polynomial, first we construct a matrix whose elements are determined by the crossing points and the direction of arcs.

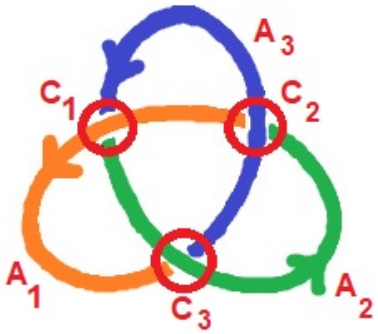

Figure 3.9: Trefoil knot with an arbitrary given direction. The crossing points are marked as C_1, C_2 and C_3, while the colored arcs are A_1, A_2, A_3. Alexander polynomial can be constructed by applying the Alexander algorithm to crossing points.

Consider the basic knot that we encountered in distance dependent SSH model. The knot as indicated before is known as the trefoil knot. With given orientation of the knot in figure 3.9, by labelling the crossing points and arcs, we could construct the fallowing matrix,

$$M = \begin{array}{c} \begin{matrix} C_1 & C_2 & C_3 \end{matrix} \\ \begin{pmatrix} 1-t & t & -1 \\ t & -1 & 1-t \\ -1 & 1-t & t \end{pmatrix} \end{array} \begin{matrix} A_1 \\ A_2 \\ A_3 \end{matrix} \tag{3.22}$$

If you cross out, one column(arc) and one row(crossing), the remaining matrix's determinant is what is known to be Alexander polynomial [4]. Depending on the row and column chosen, the results can differ by a multiplication of t^n being either positive and negative. To remove this ambiguity, the Alexander polynomial defined by diving t^n to acquire a symmetric formulation and making the highest degree variable positive. With this condition, we have the fallowing Alexander polynomial for trefoil knot [4],

$$\text{Trefoil} = t^{-1} - 1 + t. \tag{3.23}$$

Although trefoil is a relatively easy one resulting in a 3 by 3 matrix, the system gets more and more complicated when we increase the crossing points. However,

this identification allows us to find out the complex knot types which we will need in this area of research.

3.5 Klein Bottle

Now since we have a well-established knot theory, and have a system with a torus shape, can we construct another system with a different topological shape, giving another family of knots?

3.5.1 Fundamental Polygons

The torus and every other compact Riemann surface of a genus greater than 0, can be defined through fundamental polygon. The idea is a way to connect the edges of a flat surface such as a paper to obtain the topological shapes. As an example, if we connect the two opposite edges of a paper in the reverse direction, we obtain a Moebius strip (fig. 3.10) [44].

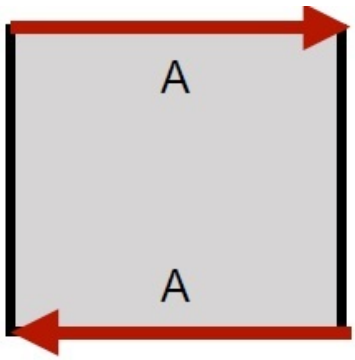

Figure 3.10: Fundamental Polygon of the Moebius strip. Edges A's can be connected to construct it.

Similarly, one could obtain the torus thorough connection of opposite edges in the same direction (fig. 3.11) [44].

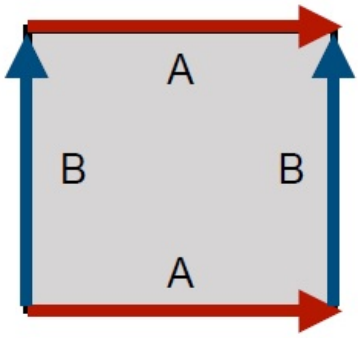

Figure 3.11: Fundamental Polygon of the Torus. Edges A's and B's can be connected to construct it. It can be represented as, $ABA^{-1}B^{-1}$.

There is another topological shape that comes to mind that has similar two parameters (p,q) parametrization as torus that is defined through the fundamental polygon as connecting the remaining edges of the Moebius strip in the same direction (fig. 3.12) [44].

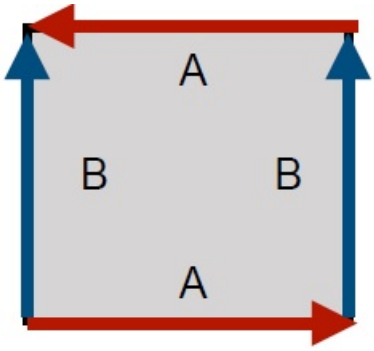

Figure 3.12: Fundamental Polygon of the Klein bottle. It can be represented as, $ABAB^{-1}$.

This shape is known as Klein bottle. Even though it is a 4-dimensional shape, there are many interpretations of it in 3D that are self-intersecting. Even though these fundamental polygons is not giving any physical insight, it makes an interesting connection to one another, since two Moebius strip can construct a Klein bottle which is easy to show with the definition of polygons and even number of Klein bottles, when it is stuck together gives torus. This gives also an interesting

question of whether these geometrical connections exist as a physical one? To understand this, we try to establish a system starting the distance vector as the parametrization of the Klein bottle.

3.5.2 Parametrizations of Klein Bottle

Klein bottle is a four-dimensional non-orientable surface. Due to the high dimensionality of the Klein bottle, there are many ways to define it. Some of the well-known parametrizations are pinched torus, figure 8 immersion, and the most commonly used 3D picture of the Klein bottle which is called the bottle shape.

Pinched Torus

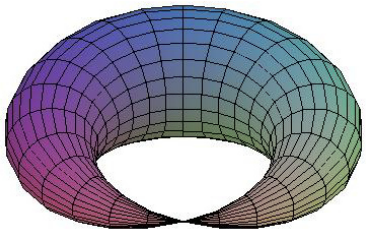

Figure 3.13: 3D picture of pinched torus. Adapted from [5].

The pinched torus parametrization can be defined through the following four dimensions [45],

$$\begin{aligned} x &= (R + r\cos\theta)\cos\phi \\ y &= (R + r\cos\theta)\sin\phi \\ z &= r\sin\theta\cos\left(\frac{\phi}{2}\right) \\ t &= r\sin\theta\sin\left(\frac{\phi}{2}\right). \end{aligned} \tag{3.24}$$

The pinched torus unlike the rest of the parametrization that will be discussed is not an immersion of the four-dimensional Klein bottle into the three-dimension.

It is just a topological equivalent of a Klein bottle that being reduced to three-dimension. Since, our distance operator is three-dimensional, in this parametrization, we have a problem of excess dimension. Since the first two dimensions are similar with torus parametrization, it is ideal to eliminate either z or t. But, on the bright side, this is the easiest parametrization of Klein bottle in terms of containing first order cosines and sines with two variables available to define hoppings.

Figure 8 Immersion

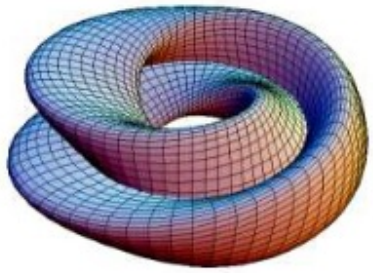

Figure 3.14: 3D picture of figure 8 immersion of Klein bottle. Adapted from [6].

The second parametrization that represents an immersion in 3D is what is called figure 8 immersion. Due to its 3D nature, the parametrization is self-intersecting. It is possible to imagine this as sticking two Mobius strip together, and where the point of sticking is the intersection. The parametrization takes the following form [6],

$$\begin{aligned} x &= (r + \cos\left(\frac{\theta}{2}\right)\sin\phi - \sin\left(\frac{\theta}{2}\right)\sin(2\phi))\cos\theta \\ y &= (r + \cos\left(\frac{\theta}{2}\right)\sin\phi - \sin\left(\frac{\theta}{2}\right)\sin(2\phi))\sin\theta \\ z &= \sin\left(\frac{\theta}{2}\right)\sin(\phi) + \cos\left(\frac{\theta}{2}\right)\sin(2\phi). \end{aligned} \tag{3.25}$$

In this parametrization, the system contains gets a little bit more complicated by introducing more terms, but still, it is a combination of sines and cosines, so one could argue it is not much different from the pinched torus parametrization. The

problem with this parametrization is having only one distance parameter that we could use as hopping. We could solve this problem by introducing another parameter to the parametrization. Similar approach was taken in [45]. Also, in the distance-dependent SSH, the parametrization does not have an exact correspondence to torus parametrization, so small deviations from the Klein bottle could potentially do not affect the topology.

Bottle Shape

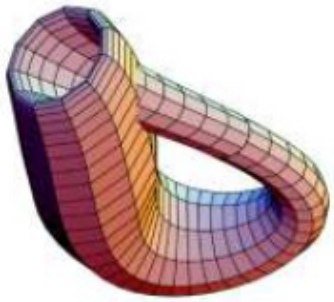

Figure 3.15: Bottle representation of the Klein bottle. Adapted from [6].

The last shape is the well-known self-intersecting picture of the Klein bottle. The parametrization takes the following form [6],

$$
\begin{aligned}
x &= -\frac{2}{15}\cos\theta\Big(3\cos\phi - 30\sin\theta + 90\cos^4\theta\sin\theta - \\
&\quad 60\cos^6\theta\sin\theta + 5\cos\theta\cos\phi\sin\theta\Big) \\
y &= -\frac{1}{15}\sin\theta\Big(3\cos\phi - 3\cos^2\theta\cos\phi - 48\cos^4\theta\cos\phi + \\
&\quad 48\cos^6\theta\cos\phi - 60\sin\theta + 5\cos\theta\cos\phi\sin(\theta) - 5\cos^3\theta\cos\phi\sin\theta \\
&\quad - 80\cos^5\theta\cos\phi\sin\theta + 80\cos^7\theta\cos\phi\sin\theta\Big) \\
z &= \frac{2}{15}\Big(3 + 5\cos\theta\sin\theta\Big)\sin\phi.
\end{aligned}
\tag{3.26}
$$

This is a rather chaotic parametrization to explain the system physically. But, it is still possible to investigate the knots. Another problem that comes with this

model is again lacking the parameters to play around with. But, this could be again fixed by introducing some parameters, that control the size of the intersection, width of the bottle, etc.

3.5.3 Klein Bottle Model

Physical Interpretation

So far, we acquired an overall idea of knot theory, topological shapes, and how to construct a Klein bottle with its parametrizations. Combining all these ideas, the first thing that should be done is to find out whether we could define a physical system that shows the Klein bottle with its distance vector. To do that, we must assign variables to the parametrizations to physical variables and work backward. Working with 3D pinched torus model by choosing the z coordinate, the most obvious choice is assigning hoppings J, $J^{'}$ to r, R and making the angles k dependent similar to the distance-dependent SSH. So, one could say θ, ϕ are $k(1-p/q)$ and kp/q respectively. Then our distance-vector becomes,

$$\begin{aligned} dx &= \left(J + J^{'}\cos\left(k - k\frac{p}{q}\right)\right)\cos\left(k\frac{p}{q}\right) \\ dy &= \left(J + J'\cos\left(k - k\frac{p}{q}\right)\right)\sin\left(k\frac{p}{q}\right) \\ dz &= J'\sin\left(k - k\frac{p}{q}\right)\cos\left(k\frac{p}{2q}\right). \end{aligned} \tag{3.27}$$

Although this distance vector looks very promising, it is easy to see that after taking the inverse Fourier transform of the system, the interpretation of the model becomes complicated. If we multiply our distance vector with the Pauli matrices, we arrive to the following hamiltonian,

$$H(k) = \begin{pmatrix} J'\sin\left(k - k\frac{p}{q}\right)\cos\left(k\frac{p}{2q}\right) & \left(J + J^{'}\cos\left(k - k\frac{p}{q}\right)\right)e^{-ik\frac{p}{q}} \\ \left(J + J^{'}\cos\left(k - k\frac{p}{q}\right)\right)e^{ik\frac{p}{q}} & -J'\sin\left(k - k\frac{p}{q}\right)\cos\left(k\frac{p}{2q}\right) \end{pmatrix}. \tag{3.28}$$

This Hamiltonian suggests the second quantization for the Hamiltonian,

$$H_k = c_k^+ c_k \frac{J'}{4} i\left(e^{-ik(1-3p/2q)} + e^{-ik(1+p/q)}\right) + c_k^+ d_k \left(Je^{-ik\frac{p}{q}} + \frac{J'}{2}e^{ik(1-2p/q)} + \frac{J'}{2}e^{-ik}\right) + d_k^+ d_k \frac{-J'}{4} i\left(e^{-ik(1-3p/2q)} + e^{-ik(1+p/q)}\right) + h.c. \tag{3.29}$$

if we assume a similar structure with the distance-dependent SSH model, the hopping locations of this system become much more complicated than expected. This Hamiltonian suggests hopping locations that are not defined with proper sites. This situation seems to be persistent in other parametrizations when a similar approach is taken, and since the pinched torus parametrization is the closest one to the torus, and has a relatively simple structure, other parametrizations of the Klein bottle seems to harder to justify with a real-life system. However, since we are working backward, there are many ways to interpret this model by changing the terms, increasing the dimension, and changing the parametrizations. Therefore, before moving on to the real-life interpretation, it is more important that we observe similar topological transitions by observing the Klein bottle knots in the system, which was the main appeal of the project.

Klein Bottle Knots

To define knots on a surface, one method that is used in the distance dependence SSH model was through changing the ratio p/q. This two parameter behavior of torus knots are well known and it is actually called (p,q) torus knot [7]. The one property of a (p,q) torus is that p represents the number of times the knot around the torus intersects the longitude line and q represents the intersection with the median of the torus (fig. 3.19).

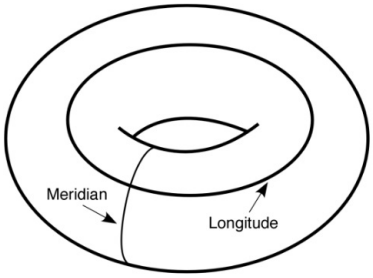

Figure 3.16: Torus. Adapted from [7].

The desire is to get similar behavior in Klein bottle knots. So, the first idea is to go through the parametrizations of the Klein bottle and see whether they correspond to a knot or not.

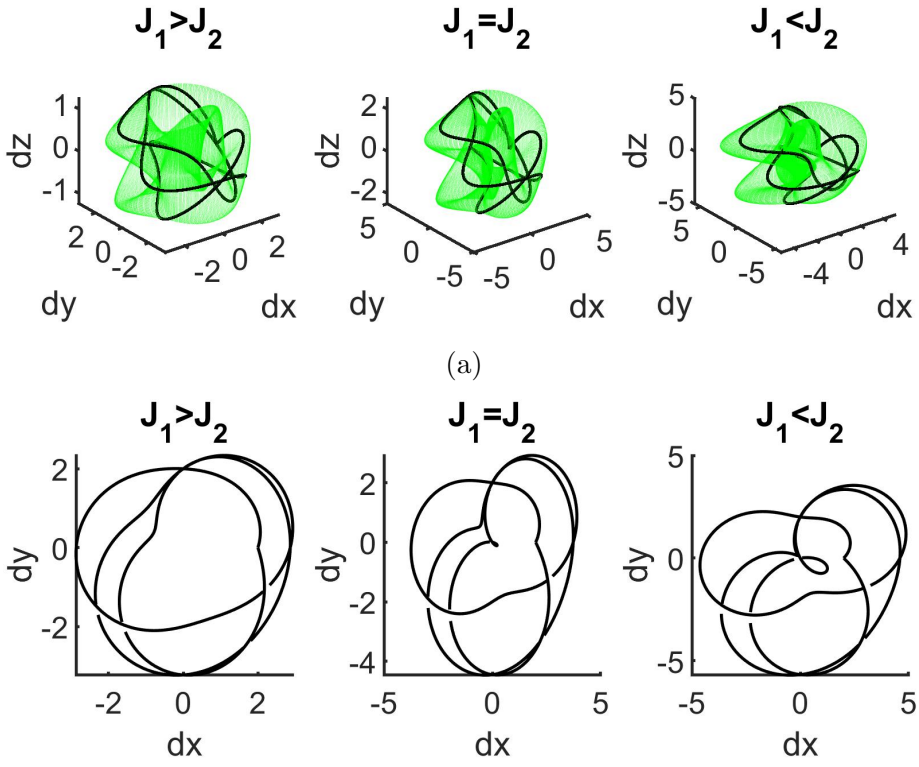

Figure 3.17: Figure 8 immersion of Klein bottle with different hopping amplitudes, where p=3 and q=5. A closed curve is traced on top of the 3D picture.

This become the first encountered problem. Due to the nature of the Klein bottle, the 3D immersion of any kind was self-intersecting. Since we go through the parametrizations of the Klein bottle, all of the curves were tracing out the 3D interpretations of the Klein bottle (fig. 3.17, 3.18, 3.20). This is the fundamental reason that we could not find a Klein bottle knot.

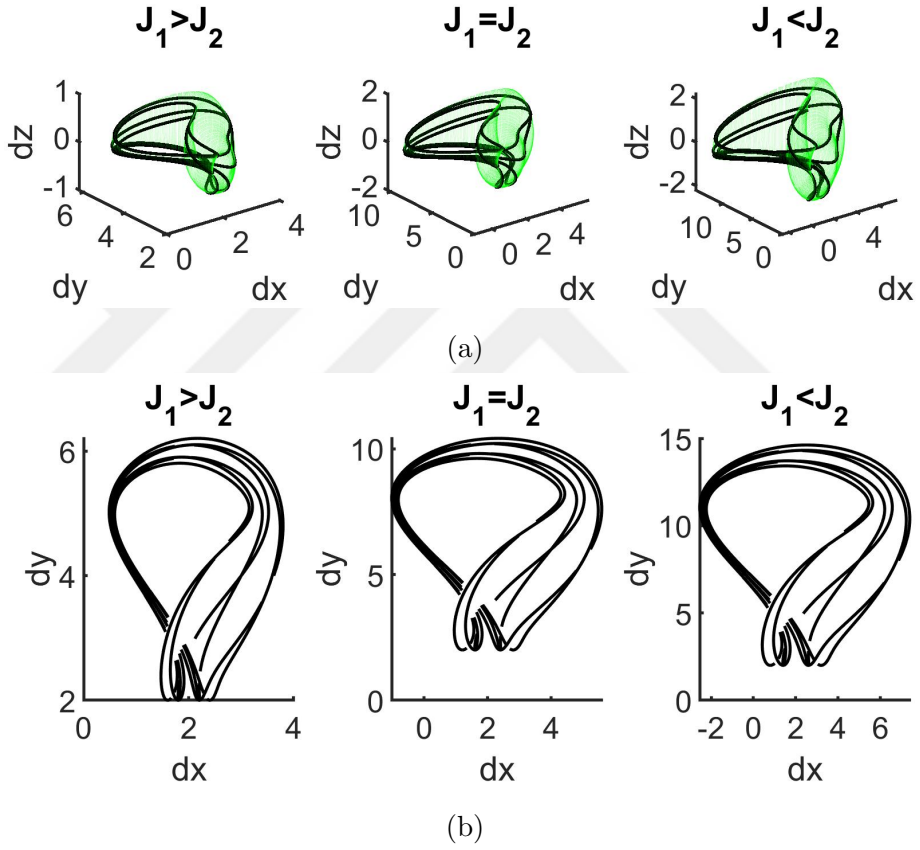

Figure 3.18: Bottle shape with different hopping amplitudes, having same parameters as figure 3.17.

The another underlying issue is the lack of symmetry in the parametrizations. As an example, although the distance vector in the distance-dependent SSH model gave torus knots and unknot depending on the hopping parameters, the standard parametrization of torus does not contain a knot transition (fig. 3.19). The

standard parametrization of a torus has the following form [46],

$$\begin{aligned} x &= (R + r\cos\theta)\cos\phi \\ y &= (R + r\cos\theta)\sin\phi \\ z &= r\sin\theta. \end{aligned} \tag{3.30}$$

Here r represents the inner radius, while R represents the outer. Due to this, when r becomes bigger than R, the torus intersects itself giving a similar problem as in the Klein bottle parametrization. This means the symmetry of hopping parameters has a significant role in defining topological transition via knots.

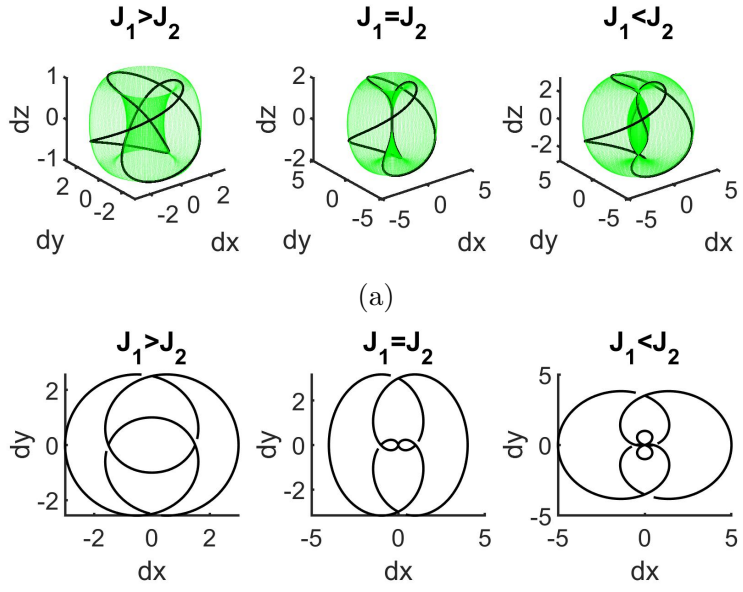

Figure 3.19: One of the torus parametrizations with different hopping amplitudes, using the same parameters p=3, q=5.

To solve these problems, we also went through the berry phase and gap closure to see what kind of system we were dealing with. For the pinched torus, we have a gap closure when the hopping parameters are equal, however, when it comes to the figure 8 immersion, the situation again becomes hard to judge. In figure 8 immersion, the gap seems to stay open when the hopping parameters are equal (fig 3.21).

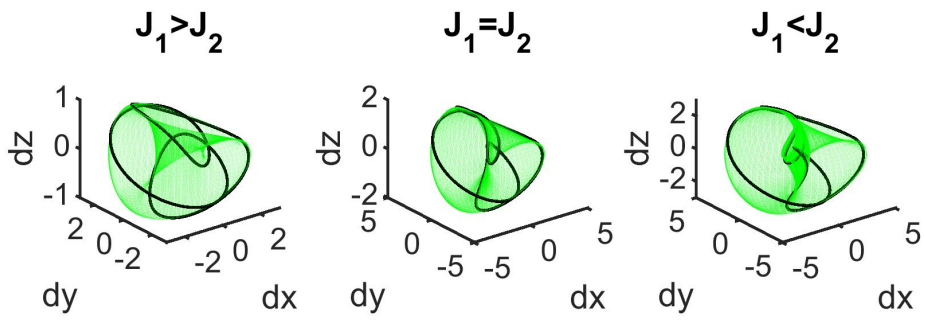

(a)

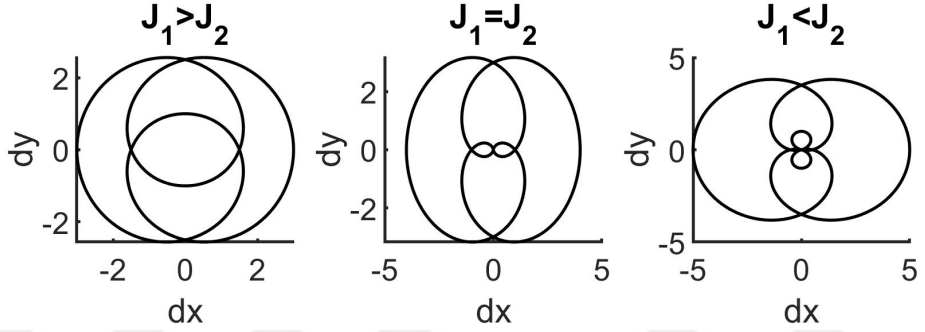

(b)

Figure 3.20: Pinched torus representation of Klein bottle with different hopping amplitudes, using the same parameters as figure 3.17.

This leads to another problematic nature of parametrizations. The final attempt to understand the behavior of these systems was through the Berry phase. The berry phase for both systems gets many values with some discontinuities (fig. 3.22).

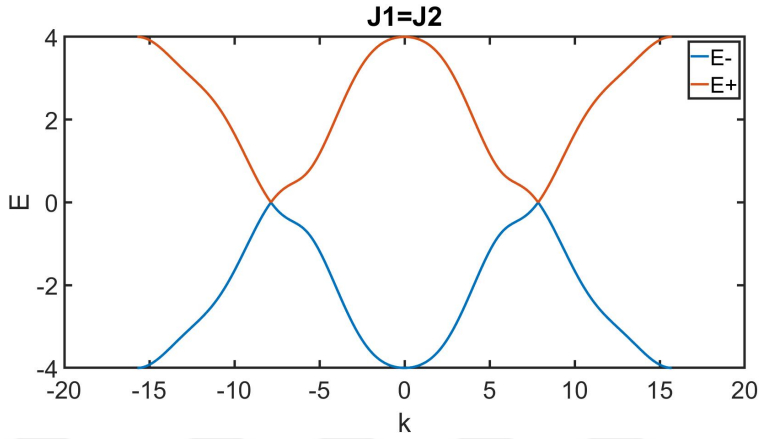

(a)

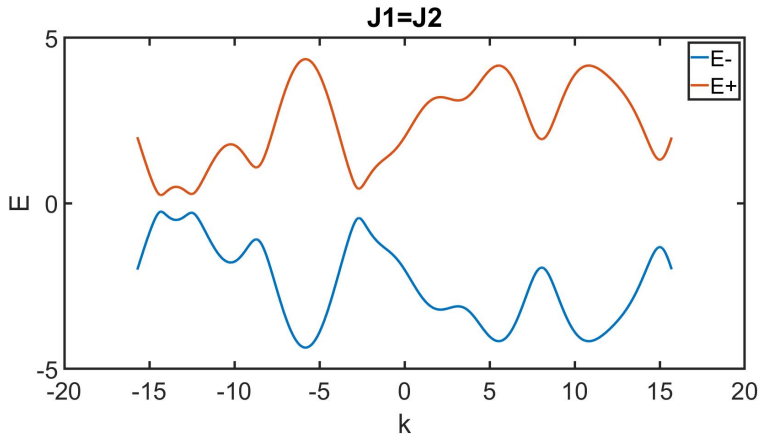

(b)

Figure 3.21: 3D pictures of a) Hopf Link and b) Unlink constructed from the fundamanetal polygons in figure 3.23b and 3.23a.

Unfortunately, none of these indicated something interesting to move on to these parameterizations. The most fundamental problem was the main appeal of the idea, which is observing a topological transition via knot theory.

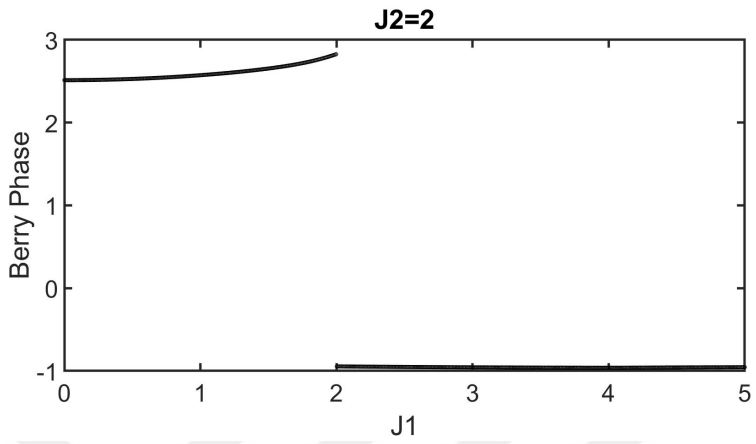

(a)

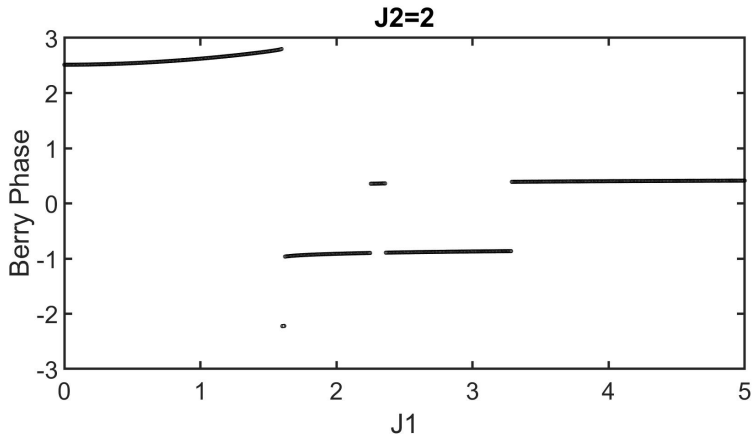

(b)

Figure 3.22: Berry phase of a) pinched torus and b) figure 8 immersion with respect to a hopping parameter J_1, while other hopping parameter J_2 kept constant.

In order to get knots on the Klein bottle, we decided on instead of focusing on the parametrizations, focusing on the knots that can be constructed through the fundamental polygons. This approach was taken in a paper written in Wooster [7]. In a similar manner, it is possible to define certain Knots on Klein bottle such as Hopf link and some interesting unknot examples such as unlink [7].

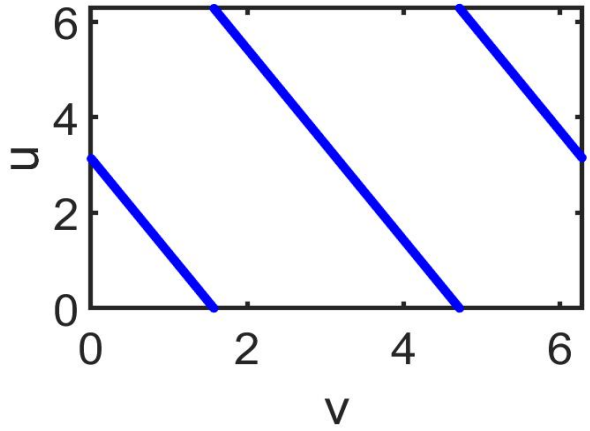

(a)

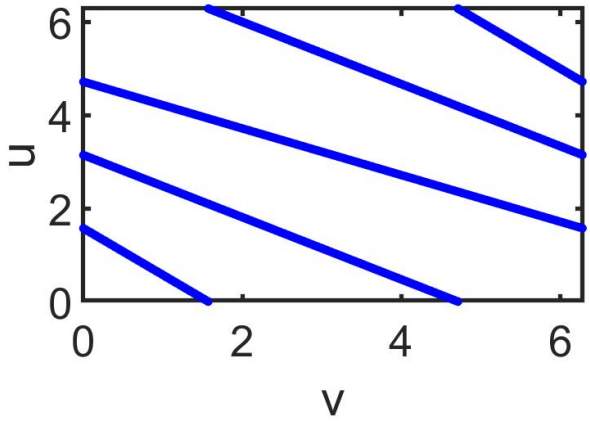

(b)

Figure 3.23: Fundamental polygons corresponding to a) unlink and b) Hopf Link.

Although these seemed to be working, again, there seems to be a possible intersection point (fig. 3.23). The reason behind the word "possible" is that the knot diagram algorithm that is constructed is a numerical approximation. This results in a visual intersection in the 3D picture(fig. 3.24), but non intersecting nature in the knot diagram (fig. 3.25). The distinction is hard to justify. Another problem with this method is that the nonparallel nature of the lines in fundamental polygons suggested different slopes for the angle variables. So, our initial suggestions about linear dependence of k must be wrong or the dimension of the system cannot be one.

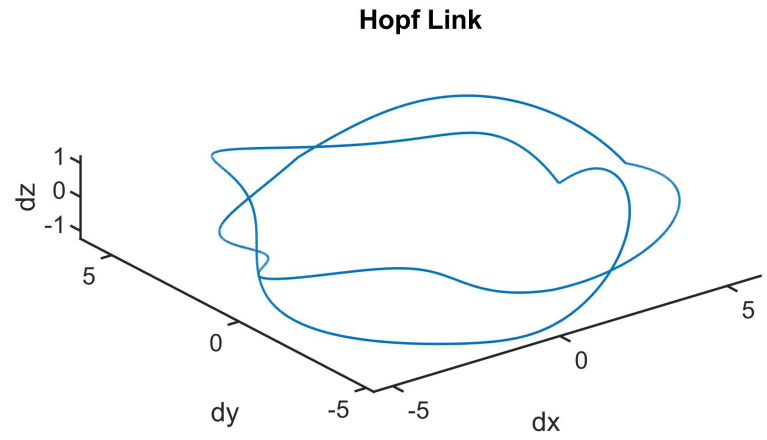

(a)

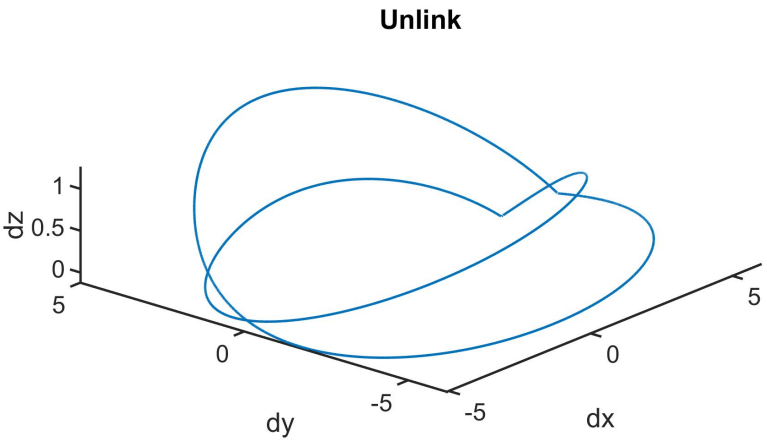

(b)

Figure 3.24: 3D pictures of a) Hopf Link and b) Unlink constructed from the fundamanetal polygons in figure 3.23.

From this point on the project needed got too complicated to deal with in a short time. How to define a proper system become much more cumbersome and the mathematics behind the Klein bottle knots required much more detailed analysis. Even though, intensive study of both physical properties like energy spectrum, topological invariant berry phase, and gap closure points, the mathematical and dimensional problems got in the way to define a proper physical system. It is definitely possible to pursue this project even further with consideration of higher dimensional spaces and with more extensive knowledge of the knot theory. But due to the time barrier, we moved on to a different system

regarding the problem of localization of an electron.

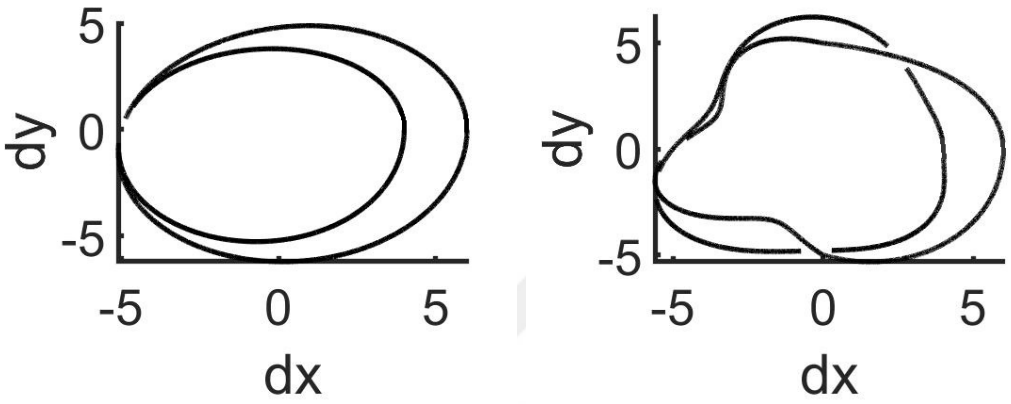

(a) (b)

Figure 3.25: Knot diagrams for a) unlink, b) Hopf link constructed from the fundamental polygons in figure 3.23.

Chapter 4

Electron Localization

As discussed in previous chapters, topological insulators had a huge impact on both experimental and theoretical physics. Even though topological insulators develop a further attraction for the insulating state of matter, the insulating and conductive state of a matter has gathered major attention for decades and still is one of the most researched areas in physics. To understand the conductivity of a system, one could say the only question that matters is whether electrons can diffuse through the system or become localized within the system. The development of localization theories began with this question and still, there is no definite solution to the problem. One of the interesting examples of localization is defined by Anderson with a disordered tight-binding system.

4.1 Anderson Localization

Anderson started his discussion with a simple question, if I put an electron to a disordered system, can I see this electron at infinity? To solve this problem first we need to construct our system. The 1D model can be expressed through the

Hamiltonian[18],

$$H = \sum_{n=1}^{L} \epsilon_n |n\rangle \langle n| + t |n\rangle \langle n+1| + h.c, \tag{4.1}$$

where t, ϵ_n are the hopping parameter and random onsite potential respectively. ϵ_n can take values between [-W, W], where W is called the disorder strength[18]. With this Hamiltonian in mind, we could tackle Anderson's question. The trivial case is when the disorder strength is 0 in the absence of disorder. In this case, the solution is plane waves, so the states are extended. But, what happens in a finite disorder strength W? The mathematics behind this is much more complicated than one expects due to the randomness of the system. For this reason, in general, a computational approach is adopted through discretization of the Schrödinger equation. For an energy eigenvalue E, one could discretize the Schrödinger equation as[18],

$$Ea_n = \epsilon_n a_n + ta_{n-1} + ta_{n+1}. \tag{4.2}$$

where a_n is the probability amplitude the wave function in nth site. We can write this equation as the matrix relation,

$$\begin{pmatrix} a_{n+1} \\ a_n \end{pmatrix} = \begin{pmatrix} \frac{E-\epsilon_n}{t} & -1 \\ 1 & 0 \end{pmatrix} \begin{pmatrix} a_n \\ a_{n-1} \end{pmatrix}. \tag{4.3}$$

The iteration matrix is called the transfer matrix. If we represent the transfer matrix of site i as T_i, it is trivial to see that[18],

$$\begin{pmatrix} a_{n+1} \\ a_n \end{pmatrix} = \prod_{i=1}^{n} T_i \begin{pmatrix} a_1 \\ a_0 \end{pmatrix}. \tag{4.4}$$

With the initial condition of initial amplitudes and energy, it is possible to evaluate the system and see the transmission and reflection rate of the system, hence understanding the localization of states through diffusion. Anderson using the discretization found out that all 1 and 2-dimensional states are localized, while in 3D there is a metal-insulator transition[18]. Understanding the inner mechanism of the transition became a subject of interest in a short time.

4.1.1 Mott's Relation

Mott, after the discovery of Anderson, to understand the localization better, decided to observe the conductivity of the system via Kuba-Greenwood formula [17]. The way Mott defined the localization was through the expectation of dc conductivity. Mott assumed, there must be a region of energies where dc conductivity is zero therefore no diffusion occurs across the system, while the opposite is true with certain energies. Mott assumed the following relation for conductivity[17],

$$\langle \sigma_E(\omega = 0) \rangle = \begin{cases} \langle \sigma_E(0) \rangle = 0 & E < E_c \\ \langle \sigma_E(0) \rangle \neq 0 & E > E_c \end{cases} \tag{4.5}$$

Mott argued that this relation of conductivity with its critical energy, suggests a jump in conductivity in E_c. This discontinuous jumped argued by contemplating the problems in continuous transition[17]. To visualize the Anderson transition, Mott also proposed the concept of mobility edge (fig 4.1)[17].

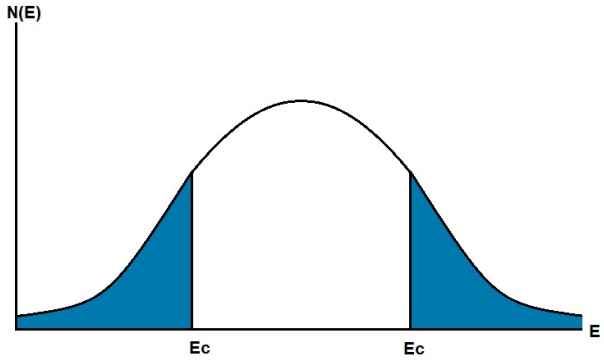

Figure 4.1: Mobility edges of the system. Conductivity is zero in shaded and non-zero in blank area.

Although the term mobility edge was used before him, the first discussion on localization was given by Mott[47]. Mott's separation of conductivity in critical values of energy can be visualized in the energy spectrum of the system. The critical values of energy create two edges for the system that moves with respect to disorder. In high disorder, limit mobility edges close and in 0 disorder the

edges open up. This is an interesting observation that can help to visualize the localization problem.

4.2 Resta's Localization

In chapter 1, we have already discussed Resta's quantity to define the position expectation in a periodic system. The central quantity that is used to define the position expectation was the folowing complex number [13],

$$z = \int_0^L e^{i\frac{2\pi}{L}x}|\psi(x)|^2 dx. \tag{4.6}$$

Apparently, this dimensionless quantity z was also a central quantity to define localization as well. It is clear from its definition is that $|z|$ cannot be larger than 1. This suggests two extrema for z, 0, and 1. If we consider a case of extreme delocalization, it is intuitive that the probability of the particle is equally distributed within the system so that $|\psi(x)|^2$ become $1/L$ [13]. Then it is clear from equation 4.6, Resta's number become 0 and in the other limit where $|\psi(x)|^2$ is a direct delta function, one acquires modulus z to be $|e^{i\frac{2\pi}{L}x_0}| = 1$. Let's consider a general case of localization, we can define the probability amplitude as [13],

$$|\psi(x)|^2 = \sum_{m=-\infty}^{\infty} n_{loc}(x - x_0 - mL), \tag{4.7}$$

where n_{loc} is some localization function that is defined with a period L. If we set x_0 to be center of the distribution, we could restrict the arbitrariness of n_{loc}, $\int_{-\infty}^{\infty} dx x n_{loc}(x) = 0$. Putting equation 4.7 into the complex number z (eq. 4.6),

$$z = \sum_{m=-\infty}^{\infty} \int_0^L e^{i\frac{2\pi}{L}x} n_{loc}(x - x_0 - mL) dx. \tag{4.8}$$

Applying change of variables $u = x - x_0 - mL$,

$$z = \sum_{m=-\infty}^{\infty} \int_{-x_0-mL}^{L-x_0-mL} e^{i\frac{2\pi}{L}x_0} e^{i\frac{2\pi}{L}u} n_{loc}(u) dx. \tag{4.9}$$

then we can express this as the Fourier transform of $n_{loc}(u)$ [13],

$$z = e^{i\frac{2\pi}{L}x_0} N_{loc}\left(\frac{-2\pi}{L}\right), \tag{4.10}$$

where $N_{loc}(\frac{-2\pi}{L})$ is the Fourier component. If the wave function is localized in real space then it is extended on the reciprocal space, then we can expend the Fourier transform expression, and using the restriction that is put to the localization function, it is possible to find that [13],

$$N_{loc}\left(\frac{-2\pi}{L}\right) = 1 - \frac{1}{2}\left(\frac{2\pi}{L}\right)^2 \int_{-\infty}^{\infty} u^2 n_{loc}(u)du + O(L^{-3}). \tag{4.11}$$

From this, it is clear that in the thermodynamic limit $L \to \infty$, $|z|$ becomes 1 for the localized state and 0 for the extended states. This is Resta's definition of localization of the electron. This definition holds true for both many-body and single-particle systems. Previous to this approach, a common approach was to solve the conductance of the system through the scaling theory of conductance.

4.3 Scaling Theory

The idea of a scaling theory, based on its name, is an approach of changing the scaling of the system while keeping the physical properties of the system intact. This systematic way to investigate the system is called the renormalization group.

4.3.1 Renormalization Group

The idea behind the renormalization group is rather simple, but the implementation could be quite different depending on the application. If our Hamiltonian is dependent on some parameters, say λ and θ, one could define a renormalization as[48],

$$H(\lambda_i, \theta_i) \to H(\lambda_f, \theta_f) \tag{4.12}$$

where i and f are initial and final parameters before and after renormalization respectively. The advantage of this method is that one could redefine a complex system into a simple one.

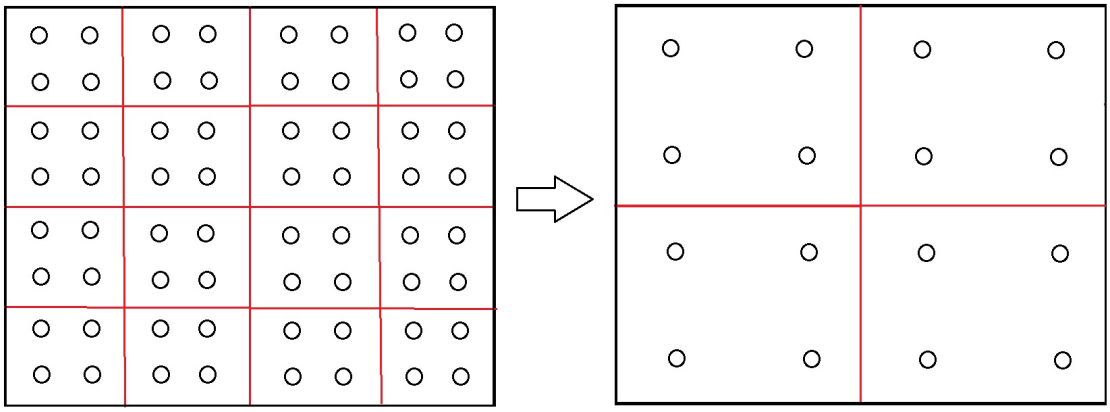

Figure 4.2: Example renormalization scheme.

But, the definition of defining this renormalization chain or flow depends on the application. In a general sense, one could say, we renormalize the system, while keeping states invariant under the scale change by adjusting the parameters of the Hamiltonian[48]. This method has also had its use in the solution of the Anderson model.

4.3.2 Scaling Theory of Localization

For the solution of the Anderson model, one of the most well-known paper is the scaling theory of localization written by E. Abrahams, P. W. Anderson, D. C. Licciardello, and T. V. Ramakrishnan. Due to these extraordinary physicists working on this single paper, it is also called the gang of four paper. They start with the idea of conductance that is developed by Thouless et al. by using the Kubo-Greenwood formula with response to the perturbation of boundary conditions on a finite sample. They define what is called to be "Thouless number" that is a function of a scale L[8],

$$g(L) = \frac{\Delta E(L)}{dE(L)/dN} = \frac{G(L)}{e^2/2\hbar}, \tag{4.13}$$

where $\Delta E(L)$ is the mean energy fluctuations when the boundary conditions are changed from periodic to antiperiodic, and $g(L)$ is the dimensionless conductance

when two hypercubes of size L^d are fitted together. From here they assume that when we fit b^d cubes of side bL together than the new $g(bL)$ is a function of our initial system (eq.4.14)[8].

$$g(bL) = f(b, g(L)). \tag{4.14}$$

If we write this relation in continuous manner,

$$\frac{L}{g}\frac{\mathrm{d}g(L)}{\mathrm{d}L} = \frac{\mathrm{d}\log g}{\mathrm{d}\log L} = \beta(g). \tag{4.15}$$

Now for the macroscopic limit, $g \gg 1$, ohm law applies, then we know the resistivity of a conductor for charge density ρ, length L and cross-section L^{d-1} is,

$$R = \rho\frac{L}{L^{d-1}} = \rho L^{2-d}. \tag{4.16}$$

Since, conductance is inverse of the resistance, we have,

$$G(L) = \sigma L^{d-2}. \tag{4.17}$$

this gives the beta function,

$$\beta_d(g(L)) = d - 2. \tag{4.18}$$

Another limit is for the small g, consequently strong disorder strength W. For this limit exponential localization can be assumed for g[8],

$$g = g_\alpha e^{-\alpha L}. \tag{4.19}$$

This gives,

$$\beta_d(g(L)) = -\alpha L = \log\left(\frac{g}{g_\alpha}\right). \tag{4.20}$$

For large and small disorder it is possible to drive the perturbation relation for beta, and arrive to the figure 4.3[8].

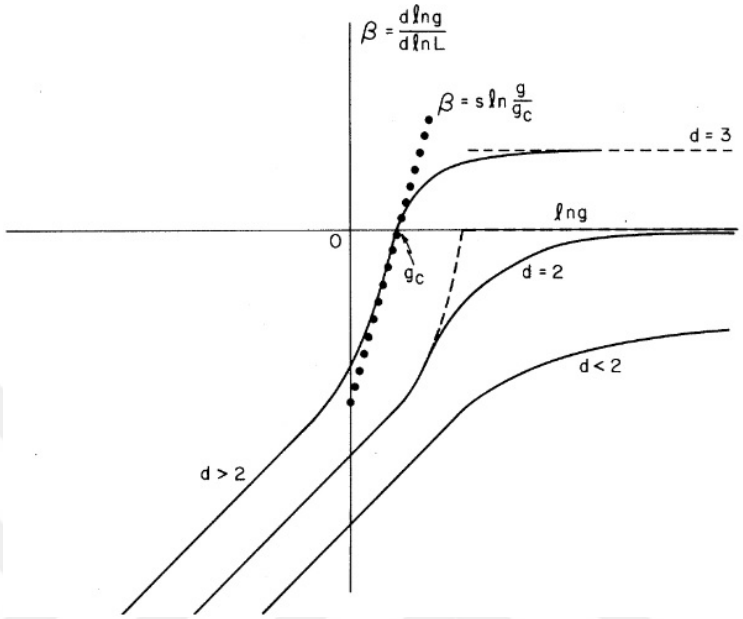

Figure 4.3: The main result of the gang of four paper. Adapted from [8].

Constructing the figure, the gang of four used an assumption on continuity of β, since β does not contain build in singularity from its definition [8]. For this reason, it would not contain sharp peaks as in the dashed line indicated in figure 4.3. This sharp transition would promote Mott's argument on sharp transition in 2D, but it is interpreted as an unphysical behavior due to continuity argument [8]. Also, they assumed that the β must be monotonic with g, since when conductance increases the scaling behavior should also increase. So, in the figure 4.3, the only singularity remains is when $g_c = 0$ in 3D. This is the point at which the system becomes size-independent, and there is a metal-insulator transition since negative scaling would mean an insulating state, while positive would indicate a conducting state. The singularity is the mobility edge that Mott proposed.

These main results suggest, MIT only occurs in 3D and there is an absence of diffusion in both 1 and 2D since β always remains negative (fig.4.3) [8]. In addition to this, the results also suggest that unlike Mott's arguments of steep jump of conductivity at the critical energy E_c, in 2D, there is a logarithmic(before) and then exponential convergence(and after the dashed line) to zero, dependent

on the size of the system, meaning there is no critical g_c in 2D [8]. Although there is no metal insulator transition in 2D, the change of its behaviour is analogical to mobility edge, so it is possible to observe a similar mobility edge behaviour in experiments[8]. These results with Resta's definition naturally beg the question, can we apply Resta's localization formula to verify the results of the gang of four?

Chapter 5

Anderson Localization with Resta's idea

To derive the connection between the gang of four and Resta's localization, we must go back to the definition of the characteristic function z_q and its cumulants in chapter 1. The second cumulant of the polarization can be written as, from the definition in equation 2.40,

$$C_2 = -\frac{L^2}{(2\pi)^2}\frac{d^2\log(z_q)}{dq^2}\bigg|_{q=0}. \tag{5.1}$$

If we take the derivative, we arrive to,

$$C_2 = -\frac{L^2}{(2\pi)^2}\left(\frac{d^2 z_q}{dq^2}\frac{1}{z_q} - \frac{dz_q}{dq}\frac{1}{{z_q}^2}\right)\bigg|_{q=0}. \tag{5.2}$$

Now we can expand this derivative using the finite difference approximation,

$$C_2 = -\frac{L^2}{(2\pi)^2}\left(\frac{z_1 + z_{-1} - 2z_0}{z_0} - \frac{z_1 - z_{-1}}{2}\frac{1}{{z_0}^2}\right). \tag{5.3}$$

Here, z_1 and z_{-1} are differ by a phase. Then, it is convenient to remove the phases of the z_q's in order to simplify the finite difference approximation. If we remove the phase of z_q, we have the following characteristic equation,

$$\tilde{z_q} = \langle\psi(x)|\exp\left(i\frac{2\pi\hat{X}}{L}q\right)|\psi(x)\rangle\exp\left(-i\,\mathrm{Im}\log\left(\langle\psi(x)|\exp\left(i\frac{2\pi\hat{X}}{L}q\right)|\psi(x)\rangle\right)\right). \tag{5.4}$$

If we expand the exponential, we can find the logarithm of the characteristic equation as,

$$\log(z_q) = \log\left(1 + i\frac{2\pi q}{L}\langle\hat{X}\rangle - \frac{1}{2}\frac{(2\pi q)^2}{L^2}\langle\hat{X}^2\rangle + ...\right) \tag{5.5}$$

Here, in the large L limit, we can treat this expansion as $\log(1+\epsilon)$. Taylor expanding this with respect to the ϵ, gives,

$$\log(z_q) = i\frac{2\pi q}{L}\langle\hat{X}\rangle - \frac{1}{2}\frac{(2\pi q)^2}{L^2}\langle\hat{X}^2\rangle + ... \tag{5.6}$$

Now, $1/L$ powers only give the mean, $1/L^2$ gives the variance, and so on. This is not surprising since the logarithm of exponential moments is known as the generating function of cumulants[49]. Then $\log(z_q)$, is

$$\log(z_q) = \sum_{n=1}^{\infty}\left(i\frac{2\pi q}{L}\right)^n\frac{C_n}{n!}. \tag{5.7}$$

Now, if we take the imaginary part of this, we exclude all the even terms. Then $\tilde{z_q}$ only consists of even terms. Giving,

$$\tilde{z_q} = \exp\left(\sum_{n=1}^{\infty}\left(i\frac{2\pi q}{L}\right)^{2n}\frac{C_{2n}}{2n!}\right). \tag{5.8}$$

From this, it is clear that the definition of the variance can again be defined through the second derivative of $\tilde{z_q}$, similar to z_q. Then using instead of z_q, $\tilde{z_q}$, we can arrive at the equation 5.3, but now, we also know that $\tilde{z_1} = \tilde{z}_{-1}$. Using this and the fact $\tilde{z_0} = 1$, we can arrive in the relation,

$$C_2 = -\frac{L^2}{2\pi^2}(\tilde{z_1} - 1). \tag{5.9}$$

Now we can use this relation and Resta's argument on how absolute of z changes with the conductivity of the system, to understand the localization of states. As mentioned before, Resta said $|z| = 1$, when the states are localized, and 0 when it is extended. Then the second cumulants should have a size scaling relation of L^2 when it is a conductor. This identification was previously used in [36]. Therefore, what we are proposing is a sort of an analog to the conductivity of a system through the Resta's quantity (eq. 5.10).

$$g(L) \to 1 - |z_1(L)|. \tag{5.10}$$

This is the first property that is used to examine the localization through Resta's quantity.

The other methodology that we will be using is based on the renormalization group. Now using the idea of renormalization, we know that the Hamiltonian of the system stays the same and the parameter of the Hamiltonian must be changed to get the same probability distribution. With this idea, it is possible to identify our changing parameter as the disorder W, while for the probability distribution, we impose the condition that

$$Z_1(L, W_i) = Z_1(L/2, W_f). \tag{5.11}$$

If we apply these steps many times, we acquire a flow diagram of disorders. This is the second criteria to verify gang of four via the modern theory of polarization.

5.1 Size Scaling Exponent

The first intuition to solve the model through its ground state. Since this is a one-electron system, it can be considered as the low-temperature limit, since the electron will occupy the lowest energy. For 1D, all states are expected to be localized. In our case, the ground state is localized except when W=0 (fig. 5.1), and interestingly the scaling goes to -0.5 in the extreme localization.

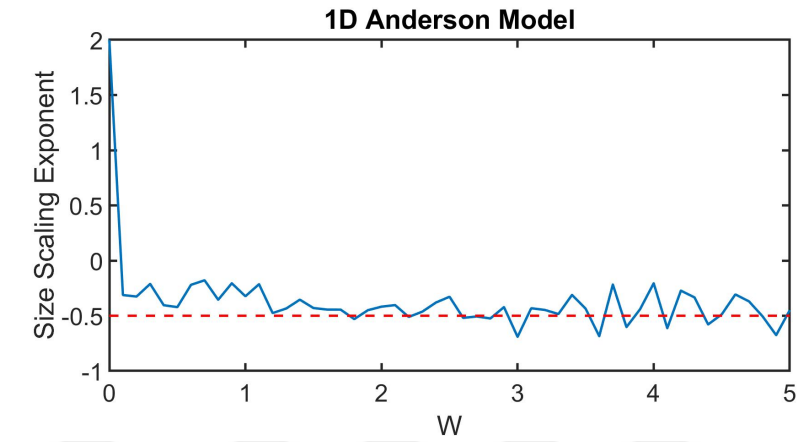

(a)

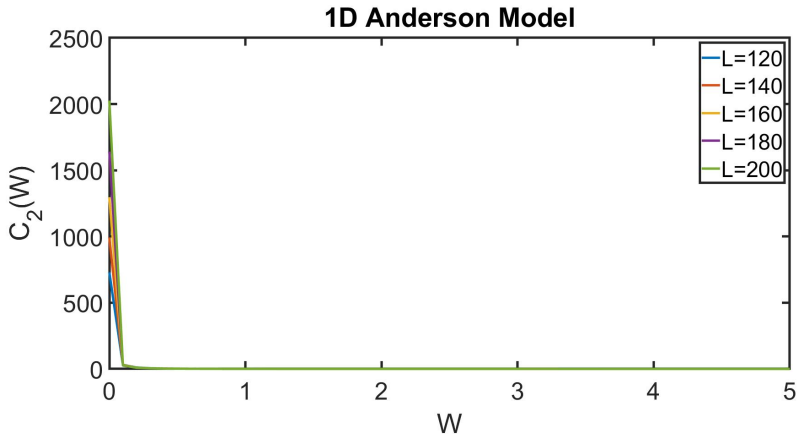

(b)

Figure 5.1: a) Ground state size scaling exponent and b) variance with respect to disorder strength for 1D Anderson model. To find the size scaling exponent a function $aL^{\gamma} + c$ is fitted to the system sizes of L= 120, 140, 160, 180, 200 with 100 realizations, where γ is the size scaling exponent.

For 2D, the situation is not so different. The transition seems to be slower and the only difference is in extreme localization. This time in the extreme localization, the system seems to have a size scaling exponent of -1 (fig. 5.2). The effect of finite system sizes can be seen through the behavior of variance when the size of the system changes. The expected behavior is when there is no disorder, the variance should go to infinity, implying a conducting state. This divergence behaviour with respect to the system size can be seen through all

dimensions (fig. 5.1, 5.2, 5.3).

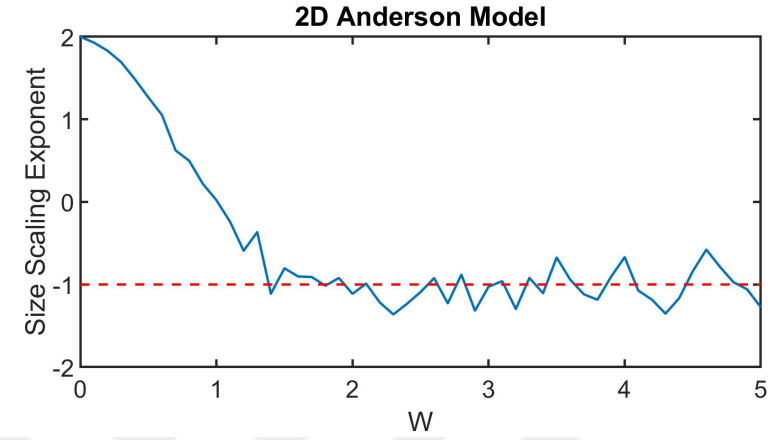

(a)

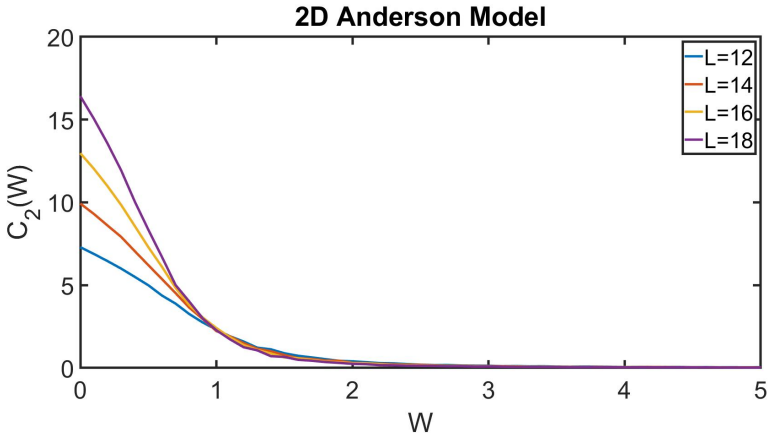

(b)

Figure 5.2: a) Ground state size scaling exponent and b) variance with respect to disorder strength for 2D Anderson model. System sizes of L= 12, 14, 16, 18, 20 with 100 realizations are used.

For 3D, it is possible to see a finite transition point through size scaling exponent, and size scaling exponent in extreme localization tends to -1.5. There seems to be a relation of $L^{-d/2}$ in extreme localization. Although we did not establish the reason, the conductive behavior with respect to the dimensionality of the system seems to be in agreement with the results of the gang of four.

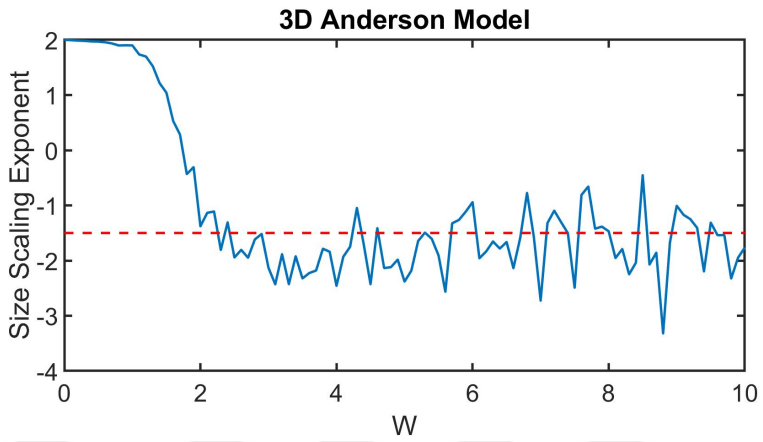

(a)

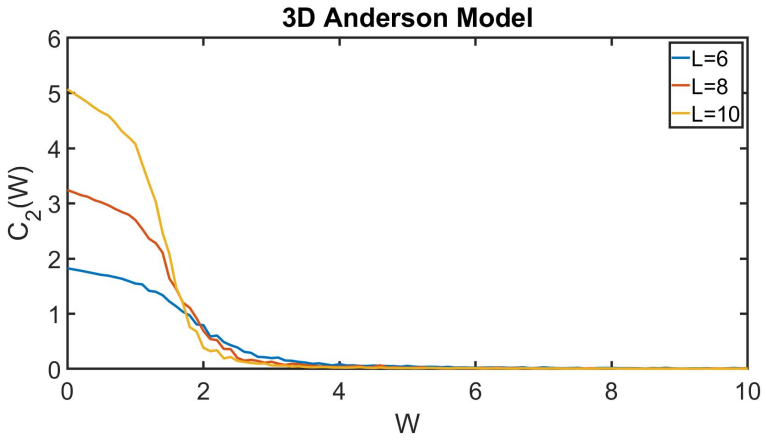

(b)

Figure 5.3: a) Ground state size scaling exponent and b) variance with respect to disorder strength for 3D Anderson model. System sizes of L= 8, 10, 12 with 100 realizations are used.

But, as discussed in chapter 3, the gang of four and others studied this system under different energies and their correspondence [8], [17]. For this reason, in order to consolidate the results, we must consider the high-temperature case, where the electron occupies the average of all eigenstates. When this is the case, for the 1D Anderson model, the transition seems to same and the behavior of the extreme localization seems to have vanished in all dimensions.

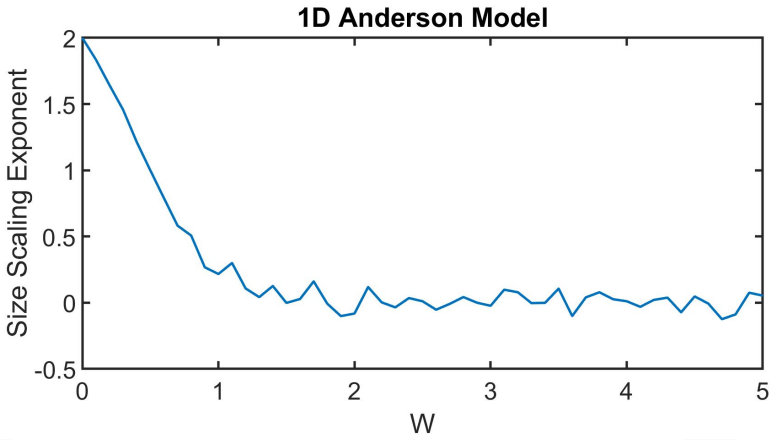

(a)

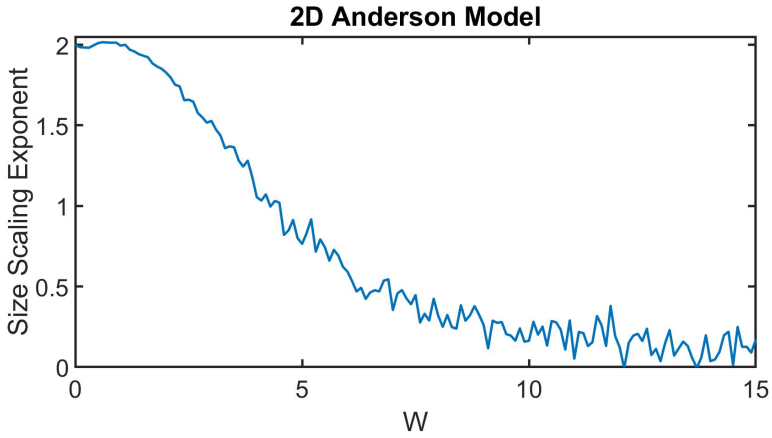

(b)

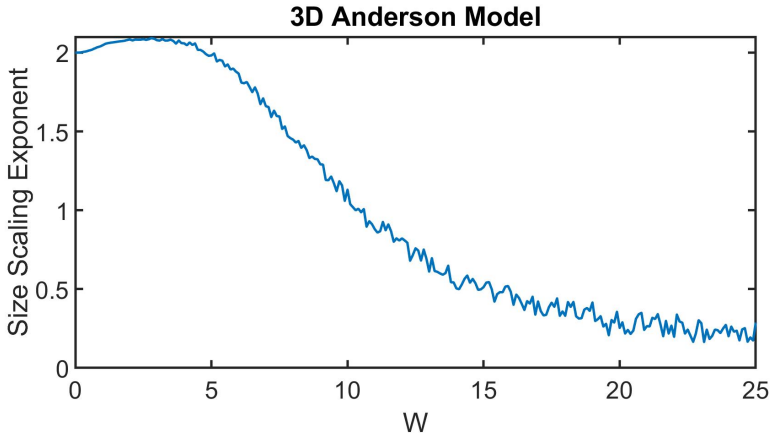

(c)

Figure 5.4: Average state size scaling exponent with respect to disorder strength for a) 1D Anderson model, where system sizes of L= 120, 140, 160, 180, 200; b) 2D Anderson model where system sizes of L= 12, 14, 16, 18, 20; c) 3D Anderson model where system sizes of L= 8, 10, 12 with 100 realizations.

For 2D, we have a metal-insulator transition in a finite disorder of $W_c \approx 1$. This clearly contradicts the result of the gang of four. But, this transition point can emerge due to having to deal with finite system sizes. The final 3D case seems to be in good agreement with the gang of four. We have a transition point around $W_c \approx 5$. We have encountered both agreement and disagreements with the gang of four. To further analyze the system, it is conventional to move into another approach which as discussed at the beginning of the chapter: the renormalization flow.

5.2 Renormalization Flow

In the renormalization scheme, as we described at the beginning of the chapter, the flow of disorder could explain the localization of the system. If the disorder flows through the infinity, then it is clear that the average state is localized. If the disorder moves towards 0, then it is well known that the state is delocalized. With these two expectations of behavior, and the algorithm of renormalization, we encountered localization in one dimension, while two fixed points in our numerical applications in 2 and 3-dimensional space.

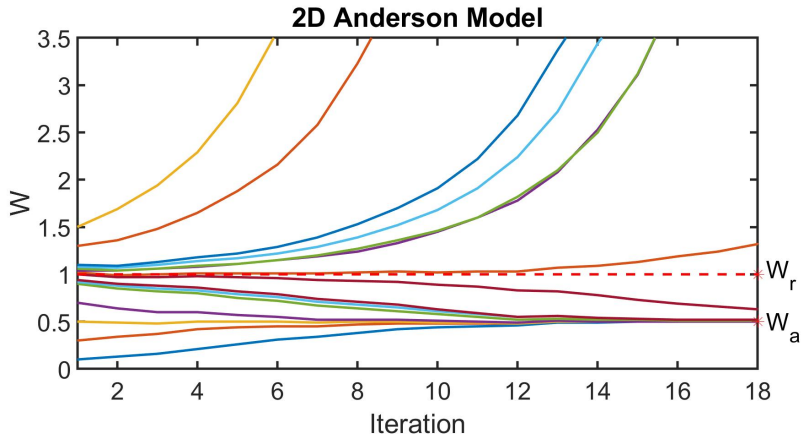

Figure 5.5: Flow diagram of 2D Anderson model of size $L = 20$ with 100 realizations.

In 2D, there seems to be a repulsive fixed point around the critical value where the systems move from one localized state to another. This critical disorder strength seems to be in agreement with our size scaling analysis. But, what is interesting is the 2D system never becomes fully localized due to some attractive fixed point. What is expected from a two-dimensional disorder system is that all states are localized. The underlying issue lying here is the limitations of computational power. Due to the necessity of finding all eigenstates and averaging them, the usual iteration algorithms to find eigenstates do not work properly. This becomes a huge issue to observe the system in the thermodynamic limit.

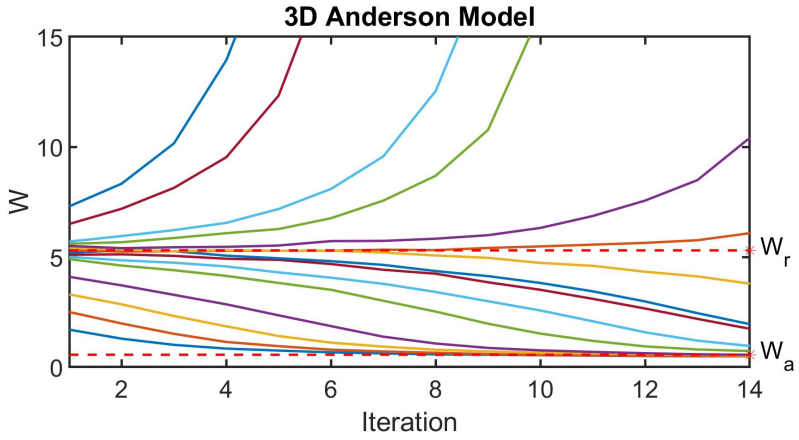

Figure 5.6: Flow diagram of 3D Anderson model of size $L = 8$ with 100 realizations.

The way we get ahead of this issue is through observation of changes of fixed points in flow diagrams. It is possible to see in both 2D and 3D, there exist two fixed points that we can define as attractive(W_a) and repulsive(W_r) fixed points (fig. 5.5, 5.6). As, the system size increases, what is observed is that, the attractive fixed points seem to be converging to 0 in both 2D and 3D which can be seen through the table 5.1. For 3D, the precision of convergence is less than 0.01, while in 2D this convergence to 0 is not easy to justify. This results in metal-insulator transition in 3D, and a possible metal-insulator transition point in 2D, where the repulsive fixed point is the point of transition.

Trials	1		2		3	
2D System	W_r	W_a	W_r	W_a	W_r	W_a
L=24(100)	1.00	0.38	0.86	0.40	0.95	0.43
L=32(50)	0.78	0.30	0.85	0.29	0.84	0.29
L=48(25)	0.69	0.19	0.75	0.17	0.69	0.16
L=64(15)	0.65	0.15	0.66	0.14	0.65	0.14
L=80(10)	0.60	0.11	0.62	0.10	0.62	0.12
L=96(5)	0.57	0.06	0.55	0.09	0.55	0.09
L=112(4)	0.51	0.08	0.53	0.07	0.56	0.06
L=128(3)	0.48	0.06	0.55	0.07	0.57	0.06

(a)

Trials	1		2		3	
3D System	W_r	W_a	W_r	W_a	W_r	W_a
L=8(100)	5.49	0.42	5.46	0.40	5.23	0.49
L=12(25)	4.96	0.30	4.87	0.28	4.73	0.25
L=16(10)	4.60	0.08	4.96	< 0.01	4.68	0.23
L=20(5)	5.05	< 0.01	4.70	< 0.01	4.58	0.05
L=24(3)	4.62	< 0.01	4.97	< 0.01	4.66	< 0.01

(b)

Table 5.1: The repulsive and attractive fixed points for the system edge size L in a) two and b) three dimensions. The number of realizations is indicated in the parenthesis.

In this case, while the 3D case is in an agreement with the gang of four, in 2D, we have an ambiguous result. If we say the attractive fixed points go to zero, to establish localization in 2D, we must see whether the repulsive fixed points go to 0 or not. The repulsive point seems to be decreasing in both 2D and 3D systems. However, due to a lack of computational power, the behavior in the thermodynamic limit is hard to judge. This ambiguity of the 2D Anderson model is a well-known issue and it is still discussed whether there is a metal-insulator transition both theoretically and experimentally [25],[24]. Only recently, in 2020,

the problems in two dimensions were overcome and the Anderson localization in 2D is observed through cold atoms [24]. The problem as stated in this paper is that the localization lengths in two dimensions are so large that, it is hard to distinguish them as localized states. Theoretical-wise, there are some papers that suggest a metal-insulator transition in two dimensional Anderson model [25]. To solve our ambiguous results in 2D, we tried to further analyze the size scaling exponents of the system with different system sizes to see if the size changes the transition point as it changes the repulsive fixed point. And, indeed this was the case (fig. 5.7).

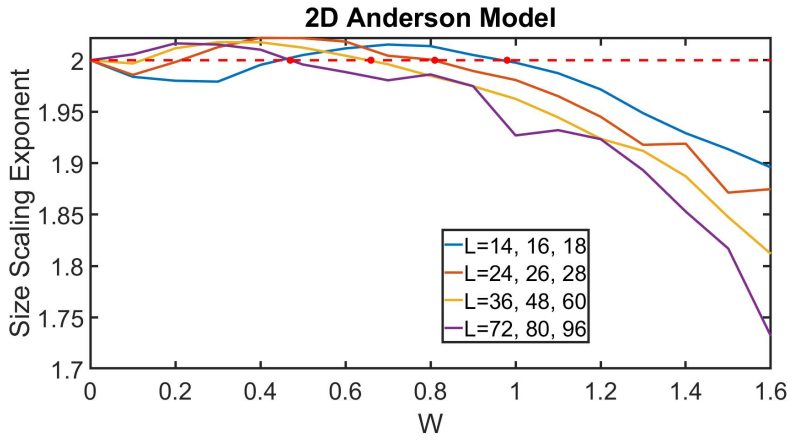

Figure 5.7: Size scaling calculations with different lengths. The red dots represents the point of transition. The systems have 1000, 500, 100 and 10 realizations of disorder, in order of smallest system size to largest system size.

As the system sizes got bigger, the transition points decreased in both 2D and 3D. When we fit the results of repulsive fixed points to a power-law function, for 3D, we acquire a constant repulsive point of 4.75 while in 2D, it is 0.29 (fig. 5.8, 5.9). Of course, these are not absolute conclusions, for 3D the results seem to be converging to a finite value, while in 2D, the situation seems harder to judge.

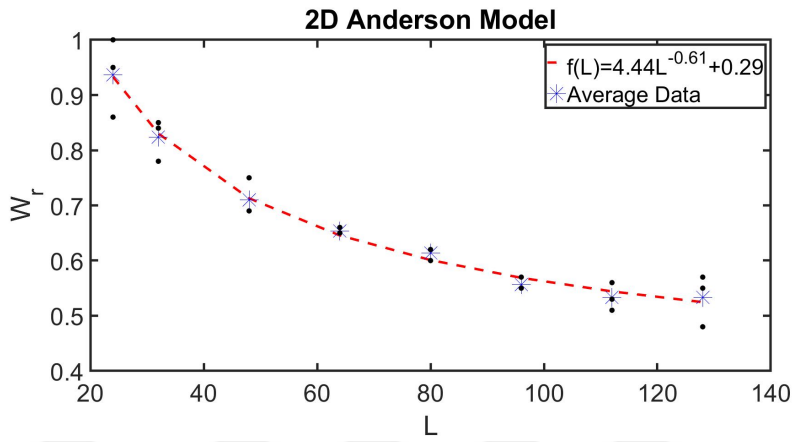

Figure 5.8: The size dependence of repulsive fixed point in 2D Anderson model. Three set of runs are averaged and fitted with a power law function.

Although the 1D and 3D results are in agreement with the expectations, the 2D results leave open a couple of possibilities. One possibility is that all states are localized in 2D meaning the fixed points becomes zero, so there is no diffusion in the system. Another possibility is that the attractive fixed point goes to zero while the repulsive fixed point goes to a constant value. This would mean in a metal-insulator transition in 2D. A final possibility is that both fixed points convergences to a finite value so that there is a transition between two localized states that we can call as weak and strong localization.

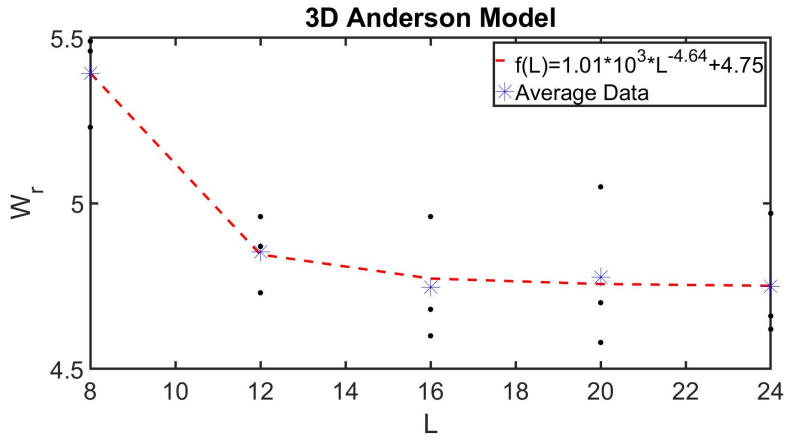

Figure 5.9: The size dependence of repulsive fixed point in 3D Anderson model. Three set of runs are averaged and fitted with a power law function.

5.2.1 Binder Cumulant and Mobility Edge

Although we established two methods at the beginning of the chapters, there are other ways to examine this problem. One of which is what is known to be Binder cumulant. Binder cumulant is known to be the ratio of forth and the second moment squared [50].

$$U = 1 - \frac{M_4}{M_2^2} \tag{5.12}$$

This cumulant is mainly used to determine the phase transitions in numerical applications [50]. In a similar method, we also examined the Binder cumulant of this system in all dimensions. For the second cumulant, it is clear that $C_2 = M_2$, from equation 5.3. For the fourth moment, we can calculate the fourth derivative finite difference as, following from binomial expansion [51],

$$M_4 = \frac{L^4}{(2\pi)^4}\Big(\tilde{z}_2 + \tilde{z}_{-2} - 4\tilde{z}_1 - 4\tilde{z}_{-1} + 6\tilde{z}_0\Big). \tag{5.13}$$

Now, using the fact $\tilde{z}_q = \tilde{z}_{-q}$ and, $\tilde{z}_0 = 1$, we get,

$$M_4 = \frac{L^4}{8\pi^4}\Big(\tilde{z}_2 - 4\tilde{z}_1 + 3\Big). \tag{5.14}$$

With this, we can calculate the Binder cumulant in our system. After the transition point, the behavior of the Binder cumulant changes, and the transition point seems to be in agreement with the previous results using the size scaling exponent (fig. 5.4, 5.10).

For a final method, we used the idea of the mobility edge to further consolidate the analogy in equation 5.10. For this, It is convenient to plot $1 - z_1$ with respect to number states. This results in, somewhat a similar picture as Mott's mobility edge. This is not a one-to-one correspondence to mobility edge, since $1 - z_1$ is a continuous function without steep jumps unlike the existence of conductivity that Mott defined in equation 4.5. z_1 takes values between 0 and 1, giving similar behaviour as conductivity, since for a perfect conductor, we expect $1 - z_1$ to be 1 and otherwise less than one. However, even though our size scaling exponent shows a conducting behavior, the resulting $1 - z_1$ and renormalization flow indicates it is not a perfect conductor for the finite periodic systems (fig. 5.11, 5.4).

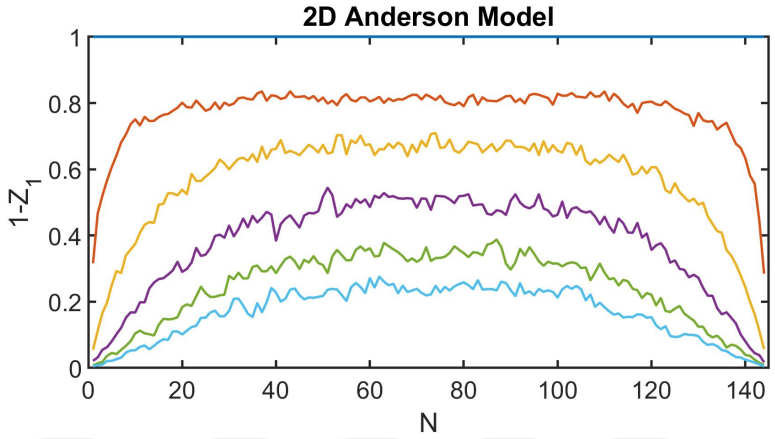

(a)

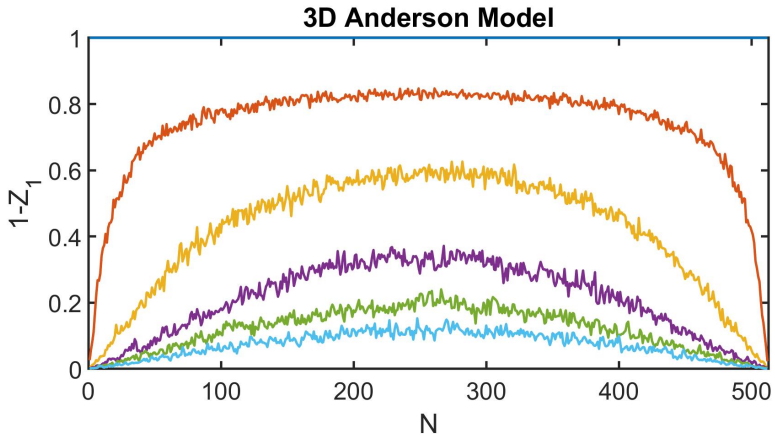

(b)

Figure 5.11: Analogical mobility edge behavior of Resta's number in a) 2D b) 3D. Different colors represents different disorder strengths. When the disorder strength is 0, the value of $1-Z_1$ becomes 1 and decreases with increasing disorder strength.

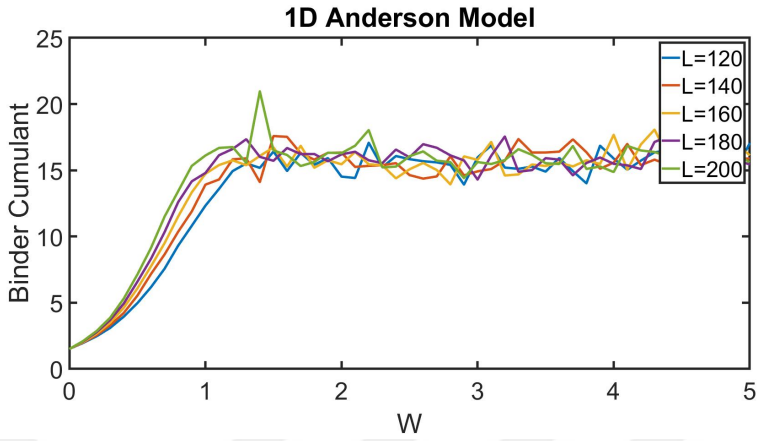

(a)

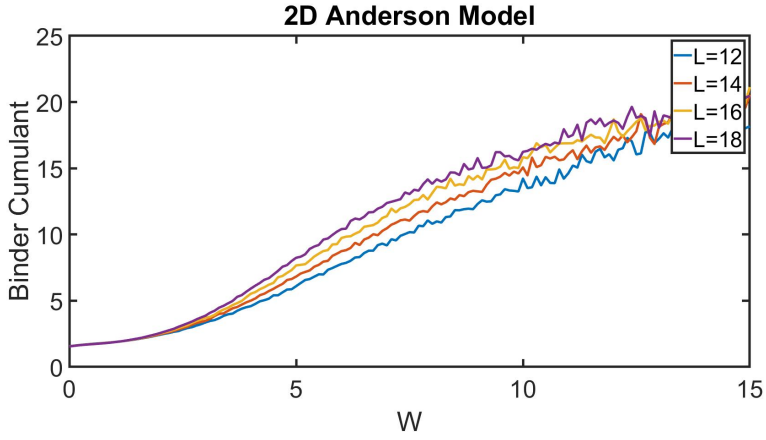

(b)

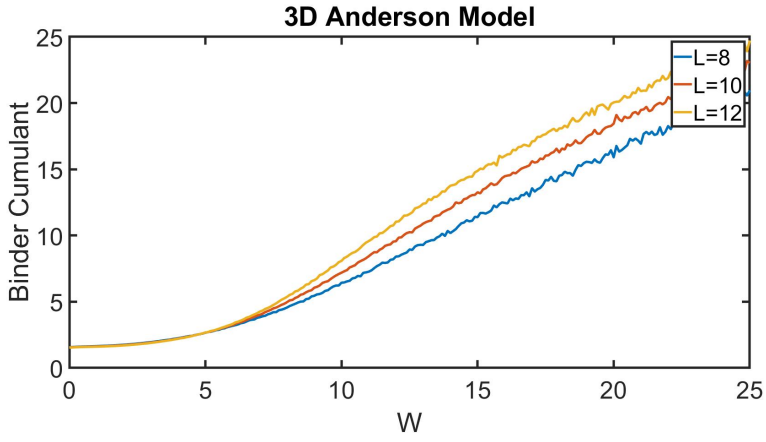

(c)

Figure 5.10: Average state Binder cumulant with respect to disorder strength for a) 1D Anderson model, where system sizes of L= 120, 140, 160, 180, 200; b) 2D Anderson model where system sizes of L= 12, 14, 16, 18, 20; c) 3D Anderson model where system sizes of L= 8, 10, 12 with 100 realizations.

Chapter 6

Conclusion

Overall, in this thesis, we went through the modern theory of polarization and applied it to topological insulators and the theory of localization. In chapter 3, we tried to create a model that has a distance vector in the shape of three-dimensional immersion of the Klein bottle, starting from a toy topological insulator model and some fundamental knowledge on knot theory. After a simple introduction to the SSH model's topological properties and symmetries, we discussed the distance-dependent SSH model and observed the emergence of knots as a way to identify topological transitions. The parameterizations of the 3D Klein bottle immersions are used as distance vector components and worked backward through to the original system. Following a similar methodology as in the distance-dependent SSH model, we proposed a rational distance change between sites. This resulted in problematic hopping locations due to the parameterizations of the Klein bottle. We tried to focus on the knots of the Klein bottle. However, since the three-dimensional Klein bottle is self-intersecting, we did not encounter a knot. To solve this problem, we tried to create links on the Klein bottle using the fundamental polygon by applying a similar approach that is used in [7]. This resulted in a Hopf link and two unlinks. However, due to the different slopes in the lines on the fundamental polygon, and possible intersection points, we could not define a one-dimensional system. In the last two chapters, we moved on to the observation of localization in the Anderson model through the modern theory of polarization.

After giving the theories on localization, we applied Resta's definition of localization to the Anderson model. Size scaling exponent of the system is observed in all three dimensions to identify metal-insulator transitions. For the low-temperature case meaning ground state, it is found out that, metal-insulator transition only occurs in 3D. For the high-temperature case, metal-insulator transition occurred in both two and three dimensions. To further examine, we proposed a renormalization group flow using polarization amplitude. This resulted in two fixed points in two and three dimensions. The attractive fixed point went to 0 in 3D, and we made an ambiguous conclusion, repulsive fixed points in 3D converge a finite value, while in 2D the behavior of fixed points seems to have multiple possible outcomes. We conclude the chapter by the discussion on the ambiguity of the two-dimensional Anderson localization and solidification of what is found by observing Binder cumulant of the system and making an analog to the mobility edge.

Bibliography

[1] P. W. Anderson, "Nobel lecture — nobelprize.org," 1977. `https://www.nobelprize.org/prizes/physics/1977/anderson/lecture/`, Online; accessed 25-November-2021.

[2] S. Ryu, A. P. Schnyder, A. Furusaki, and A. W. Ludwig, "Topological insulators and superconductors: tenfold way and dimensional hierarchy," *New Journal of Physics*, vol. 12, no. 6, p. 065010, 2010.

[3] B. Hetényi, Y. Pulcu, and S. Doğan, "Calculating the polarization in bipartite lattice models: Application to an extended su-schrieffer-heeger model," *Physical Review B*, vol. 103, no. 7, p. 075117, 2021.

[4] C. C. Adams, *The knot book*. American Mathematical Soc., 1994.

[5] W. F. by Night, "Pinched torus — Wikipedia, the free encyclopedia," 2010. `https://en.wikipedia.org/wiki/Pinched_torus`, Online; accessed 25-October-2021.

[6] G. Franzoni, "The klein bottle in its classical shape: a further step towards a good parametrization," *arXiv preprint arXiv:0909.5354*, 2009.

[7] L. Catalano, D. Freund, R. Ruzvidzo, J. Bowen, and J. Ramsay, "A preliminary study of klein knots," in *Proceedings of the Midstates Conference for Undergraduate Research in Computer Science and Mathematics at Wittenberg University*, pp. 10–17, 2010.

[8] E. Abrahams, P. Anderson, D. Licciardello, and T. Ramakrishnan, "Scaling theory of localization: Absence of quantum diffusion in two dimensions," *Physical Review Letters*, vol. 42, no. 10, p. 673, 1979.

[9] N. A. Spaldin, "A beginner's guide to the modern theory of polarization," *Journal of Solid State Chemistry*, vol. 195, pp. 2–10, 2012.

[10] R. Resta, "Theory of the electric polarization in crystals," *Ferroelectrics*, vol. 136, no. 1, pp. 51–55, 1992.

[11] R. King-Smith and D. Vanderbilt, "Theory of polarization of crystalline solids," *Physical Review B*, vol. 47, no. 3, p. 1651, 1993.

[12] R. Resta, "Quantum-mechanical position operator in extended systems," *Physical Review Letters*, vol. 80, no. 9, p. 1800, 1998.

[13] R. Resta and S. Sorella, "Electron localization in the insulating state," *Physical Review Letters*, vol. 82, no. 2, p. 370, 1999.

[14] R. Resta, "Manifestations of berry's phase in molecules and condensed matter," *Journal of Physics: Condensed Matter*, vol. 12, no. 9, p. R107, 2000.

[15] P. W. Anderson, "Absence of diffusion in certain random lattices," *Physical review*, vol. 109, no. 5, p. 1492, 1958.

[16] B. Kramer and A. MacKinnon, "Localization: theory and experiment," *Reports on Progress in Physics*, vol. 56, no. 12, p. 1469, 1993.

[17] N. Mott, "Conduction in non-crystalline systems: I. localized electronic states in disordered systems," *Philosophical Magazine*, vol. 17, no. 150, pp. 1259–1268, 1968.

[18] D. J. Thouless, "Electrons in disordered systems and the theory of localization," *Physics Reports*, vol. 13, no. 3, pp. 93–142, 1974.

[19] F. J. Wegner, "Electrons in disordered systems. scaling near the mobility edge," *Zeitschrift für Physik B Condensed Matter*, vol. 25, no. 4, pp. 327–337, 1976.

[20] A. MacKinnon and B. Kramer, "One-parameter scaling of localization length and conductance in disordered systems," *Physical Review Letters*, vol. 47, no. 21, p. 1546, 1981.

[21] A. MacKinnon, "The calculation of transport properties and density of states of disordered solids," *Zeitschrift für Physik B Condensed Matter*, vol. 59, no. 4, pp. 385–390, 1985.

[22] J. Billy, V. Josse, Z. Zuo, A. Bernard, B. Hambrecht, P. Lugan, D. Clément, L. Sanchez-Palencia, P. Bouyer, and A. Aspect, "Direct observation of anderson localization of matter waves in a controlled disorder," *Nature*, vol. 453, no. 7197, pp. 891–894, 2008.

[23] T. Schwartz, G. Bartal, S. Fishman, and M. Segev, "Transport and anderson localization in disordered two-dimensional photonic lattices," *Nature*, vol. 446, no. 7131, pp. 52–55, 2007.

[24] D. H. White, T. A. Haase, D. J. Brown, M. D. Hoogerland, M. S. Najafabadi, J. L. Helm, C. Gies, D. Schumayer, and D. A. Hutchinson, "Observation of two-dimensional anderson localisation of ultracold atoms," *Nature communications*, vol. 11, no. 1, pp. 1–8, 2020.

[25] I. Suslov, "Possibility of the 2d anderson transition and generalized lyapunov exponents," *arXiv preprint arXiv:0801.4686*, 2008.

[26] K. v. Klitzing, G. Dorda, and M. Pepper, "New method for high-accuracy determination of the fine-structure constant based on quantized hall resistance," *Physical review letters*, vol. 45, no. 6, p. 494, 1980.

[27] B. Simon, "Holonomy, the quantum adiabatic theorem, and berry's phase," *Physical Review Letters*, vol. 51, no. 24, p. 2167, 1983.

[28] M. V. Berry, "Quantal phase factors accompanying adiabatic changes," *Proceedings of the Royal Society of London. A. Mathematical and Physical Sciences*, vol. 392, no. 1802, pp. 45–57, 1984.

[29] F. D. M. Haldane, "Model for a quantum hall effect without landau levels: Condensed-matter realization of the" parity anomaly"," *Physical review letters*, vol. 61, no. 18, p. 2015, 1988.

[30] A. Kitaev, "Periodic table for topological insulators and superconductors," in *AIP conference proceedings*, vol. 1134, pp. 22–30, American Institute of Physics, 2009.

[31] C.-K. Chiu, J. C. Teo, A. P. Schnyder, and S. Ryu, "Classification of topological quantum matter with symmetries," *Reviews of Modern Physics*, vol. 88, no. 3, p. 035005, 2016.

[32] A. P. Schnyder, S. Ryu, A. Furusaki, and A. W. Ludwig, "Classification of topological insulators and superconductors in three spatial dimensions," *Physical Review B*, vol. 78, no. 19, p. 195125, 2008.

[33] M. Kline, "Euler and infinite series," *Mathematics Magazine*, vol. 56, no. 5, pp. 307–315, 1983.

[34] R. Resta and D. Vanderbilt, "Theory of polarization: a modern approach," *Physics of Ferroelectrics*, pp. 31–68, 2007.

[35] C. E. Dreyer, M. Stengel, and D. Vanderbilt, "Current-density implementation for calculating flexoelectric coefficients," *Physical Review B*, vol. 98, no. 7, p. 075153, 2018.

[36] B. Hetényi and B. Dóra, "Quantum phase transitions from analysis of the polarization amplitude," *Physical Review B*, vol. 99, no. 8, p. 085126, 2019.

[37] M. E. Cage, K. Klitzing, A. Chang, F. Duncan, M. Haldane, R. Laughlin, A. Pruisken, and D. Thouless, *The quantum Hall effect*. Springer Science & Business Media, 2012.

[38] J. K. Asbóth, L. Oroszlány, and A. Pályi, "A short course on topological insulators," *Lecture notes in physics*, vol. 919, p. 166, 2016.

[39] C. L. Kane, "Topological band theory and the 2 invariant," in *Contemporary Concepts of Condensed Matter Science*, vol. 6, pp. 3–34, Elsevier, 2013.

[40] A. W. Ludwig, "Topological phases: classification of topological insulators and superconductors of non-interacting fermions, and beyond," *Physica Scripta*, vol. 2016, no. T168, p. 014001, 2015.

[41] B. A. Bernevig, *Topological insulators and topological superconductors*. Princeton university press, 2013.

[42] C. Kittel, "Introduction to solid state physics," 1976.

[43] R. Whitty, "Some comments on multiple discovery in mathematics," *arXiv preprint arXiv:1412.3718*, 2014.

[44] C. Breen, "The classification of surfaces."

[45] R. Ferréol, "Klein bottle," 2017. `https://mathcurve.com/surfaces.gb/klein/klein.shtml`, Online; accessed 25-October-2021.

[46] C. Oberti and R. L. Ricca, "On torus knots and unknots," *Journal of Knot Theory and Its Ramifications*, vol. 25, no. 06, p. 1650036, 2016.

[47] N. Mott, "The mobility edge since 1967," *Journal of Physics C: Solid State Physics*, vol. 20, no. 21, p. 3075, 1987.

[48] L. P. Kadanoff, "Scaling laws for ising models near t c," *Physics Physique Fizika*, vol. 2, no. 6, p. 263, 1966.

[49] M. Kardar, *Statistical physics of particles*. Cambridge University Press, 2007.

[50] K. Binder and D. W. Heermann, "Theoretical foundations of the monte carlo method and its applications in statistical physics," in *Monte Carlo Simulation in Statistical Physics*, pp. 5–67, Springer, 2010.

[51] B. Fornberg, "Generation of finite difference formulas on arbitrarily spaced grids," *Mathematics of computation*, vol. 51, no. 184, pp. 699–706, 1988.